



# $^{87}\text{Sr}/^{86}\text{Sr}$ , Ca/Sr, and Ge/Si ratios as tracers of solute sources and biogeochemical cycling at a temperate forested shale catchment, central Pennsylvania, USA



Katherine Meek <sup>a,\*</sup>, Louis Derry <sup>a</sup>, Jed Sparks <sup>b</sup>, Lawrence Cathles <sup>a</sup>

<sup>a</sup> Department of Earth and Atmospheric Sciences, Snee Hall, Cornell University, Ithaca, NY 14853, USA

<sup>b</sup> Department of Ecology and Evolutionary Biology, Corson/Mudd Hall, Cornell University, Ithaca, NY 14853, USA

## ARTICLE INFO

### Article history:

Received 30 September 2015

Received in revised form 22 April 2016

Accepted 25 April 2016

Available online 29 April 2016

### Keywords:

Sr isotopes

Trace elements

Fractionation

Critical zone science

Biogeochemical cycling

## ABSTRACT

Plant uptake and biological cycling processes are commonly the largest flux of nutrients in terrestrial ecosystems. Hydrologic and other losses are offset by inputs from atmospheric deposition and weathering. This multi-tracer study investigates these effects using  $^{87}\text{Sr}/^{86}\text{Sr}$ , Ca/Sr, and Ge/Si ratios from solid (soil profiles and bedrock), biological (leaves and sap waters), and water (pore-, ground-, stream-waters) samples to study Ca, Sr, Ge, and Si sources and cycling in a forest catchment underlying gray shale in the temperate climate of central Pennsylvania. Leaves and sap waters were found to have similar Ge/Si ratios  $<1 \mu\text{mol/mol}$  which is consistent with biological fractionation occurring at the root–soil water interface. Ge/Si ratios in soil porewaters were higher near the surface and increased over the growing season suggesting plant preferential uptake of Si over Ge. Ca/Sr ratios in oak leaves ( $1360 \pm 40 \text{ mol/mol}$ ) were significantly higher than those in maple leaves ( $650 \pm 20 \text{ mol/mol}$ ). Ca/Sr ratios were also generally higher in leaves than in sap waters which are consistent with preferential Sr adsorption or Sr uptake during transpiration.  $^{87}\text{Sr}/^{86}\text{Sr}$  ratios in both leaves and sap waters were similar for a given site implying that trees access similar pools of Sr and Ca, although there are site-to-site differences. Additionally,  $^{87}\text{Sr}/^{86}\text{Sr}$  ratios in plant tissues were most similar to shallow pore waters (0–50 cm) suggesting that mineral nutrients are obtained by trees from the near sub-surface.  $^{87}\text{Sr}/^{86}\text{Sr}$  ratios in soil solutions from ridgetop and swale sites are best explained by mixing Sr derived from shale and atmospheric deposition. Valley bottom soil reservoirs and stream and groundwater samples include Sr and Ca derived from dissolution of two isotopically distinct generations of carbonates. A preliminary estimate of the Sr and Ca stream fluxes and isotopic mass balances imply propagation of a carbonate weathering front of ca.  $300 \text{ m Myr}^{-1}$ , a value larger than previously reported for regolith weathering advance rates calculated based on cosmogenic nuclides and U-series isotopes. The data for Ca, Sr, Si, and Ge in soil, soil solutions, and stream waters reflect the interaction of slower weathering processes with rapid, biologically driven cycling between soils and biomass.

© 2016 Elsevier B.V. All rights reserved.

## 1. Introduction

Multi-tracer studies have long employed isotopes and trace element data to investigate weathering and solute transport in watersheds (Aberg et al., 1989; Murnane and Stallard, 1990; Bailey et al., 1996; Kurtz et al., 2002; Derry et al., 2006; Pett-Ridge et al., 2009). In this study, a combination of  $^{87}\text{Sr}/^{86}\text{Sr}$ , Ca/Sr, and Ge/Si ratios is used to identify solute sources and investigate biogeochemical cycling processes at the Susquehanna Shale Hills Critical Zone Observatory (SSHCZO). As a small watershed with a relatively homogenous geology, ecology, and land use history, the SSHCZO serves as an ideal setting to explore

these questions and provide insight that future biogeochemical studies can expand on.

Conventionally, measured strontium isotope ratios are invariant over weathering timescales and exhibit negligible fractionation during biogeochemical processes such as plant uptake, evapotranspiration, and mineral dissolution and precipitation. As a consequence,  $^{87}\text{Sr}/^{86}\text{Sr}$  ratios serve as conservative tracers for the investigation of solute source materials, flow pathways, and mixing processes in watersheds (Bain and Bacon, 1994; Aberg, 1995; Kennedy et al., 1998; Hogan and Blum, 2002; Shand et al., 2007). Sr is only a minor constituent of soils, rocks, and plants and is not considered to be an important plant nutrient or weathering product (Capo et al., 1998). However, Sr exhibits similar chemical behavior to Ca (i.e., similar ionic charge, radius, and electron configuration) and as such,  $^{87}\text{Sr}/^{86}\text{Sr}$  and Ca/Sr ratios can be combined to investigate Ca sources in terrestrial systems (Miller et al., 1993;

\* Corresponding author.

E-mail address: [kem269@cornell.edu](mailto:kem269@cornell.edu) (K. Meek).

Bailey et al., 1996; Blum et al., 2002; Kennedy et al., 2002; Bullen and Bailey, 2005; Pett-Ridge et al., 2009; Belanger et al., 2012).

Ca is an essential macronutrient involved in several important aspects of plant function including cell wall stabilization, stomatal regulation, and intercellular signaling (McLaughlin and Wimmer, 1999; White and Broadley, 2003; Marschner, 2012). Ca transport through the xylem largely occurs passively via apoplastic (i.e., through cell walls and intercellular spaces rather than through living cells) pathways that are heavily influenced by levels of plant transpiration (Clarkson, 1984; White, 2001; White et al., 2002). As an immobile element, Ca is not translocated to other plant tissues after assimilation into leaf tissue. En route through the xylem from root to leaf tissues, divalent cations are involved in cation exchange reactions at negatively charged sites on the walls of xylem vessels and surrounding tissues. Sr is generally retained by cation exchange sites to a greater degree than Ca with increased translocation of Ca relative to Sr observed in foliage (Veresoglou et al., 1996; Poszwa et al., 2000; Dasch et al., 2006; Blum et al., 2008, 2012; Pett-Ridge et al., 2009; Funk and Amatangelo, 2013). However, heterogeneity in the distribution and availability of Ca in the forest floor (Bullen and Bailey, 2005) and/or soil reservoirs may affect the accessibility of Ca by plants at the catchment level. As such, Sr isotopes can be used to provide an indication of sources from which plants are acquiring Sr (and by inference, Ca).

In contrast to Sr isotopes, Ge/Si ratios undergo fractionation during weathering and plant uptake processes with Ge enriched in secondary minerals (Murnane and Stallard, 1990; Kurtz et al., 2002; Scribner et al., 2006) and depleted in biogenic materials (Derry et al., 2005; Blecker et al., 2007; Delvigne et al., 2009) relative to parent bedrock. Specifically, during mineral weathering, Ge is retained to a greater degree than Si in secondary phases (i.e., secondary soil aluminosilicates) that are known to contain weakly polymerized silicate tetrahedra (Murnane and Stallard, 1990). In the case of plant uptake, Ge is discriminated against relative to Si resulting in lower Ge/Si ratios in leaf phytoliths compared to soil minerals and porewaters (Blecker, 2005; Derry et al., 2005; Garvin, 2006; Blecker et al., 2007; Delvigne et al., 2009). Often considered a “pseudo-isotope” of Si, Ge displays several chemical similarities to Si including its nature as a group IV element, a similar ionic radius (Ge: 3.9 Å versus Si: 2.6 Å, Shannon, 1976), a similar tetrahedral bond length (Ge–O: 1.75 Å versus Si–O: 1.64 Å, Martin et al., 1996), and an identical outer electron configuration (Kurtz and Derry, 2004). These chemical properties enable Ge to substitute for Si at tetrahedral sites of silicate minerals (Goldschmidt, 1958; Bernstein, 1985). Accordingly, Ge/Si ratios serve as particularly useful tracers of silicate weathering processes (Murnane and Stallard, 1990; Kurtz et al., 2002; Derry et al., 2006; Scribner et al., 2006; Lugolobi et al., 2010) and Si pathways in the soil–plant system.

Si is a “pseudo-essential” nutrient whose presence in plant tissues often promotes growth and vitality (Epstein, 1994). As a structural component in cell walls, Si has been shown to facilitate light interception and photosynthesis as demonstrated by observations of more upright posture in plants abundantly supplied with Si (Raven, 1983). Additionally, deposition of Si in plant tissues generates a tough outer layer to provide protection against herbivory and infection (Epstein, 1999; Fauteux et al., 2005). Furthermore, Si's presence in plant tissue is responsible for the sequestration of Al, a known plant toxin, in aluminosilicate and hydroxylaluminosilicate complexes (Cocker et al., 1998; Doucet et al., 2001). Si has also been implicated in immobilizing Fe and Mn by transforming them to less toxic forms in plant roots (Ma and Takahashi, 1990).

Plant roots acquire Si from the soil solution as monosilicic acid ( $\text{H}_4\text{SiO}_4$ ). Monosilicic acid is then transferred to stem and leaf components of the plant through the transpiration stream where it precipitates as amorphous opal phytoliths (Opal A:  $\text{SiO}_2 \cdot n\text{H}_2\text{O}$ ) (Jones and Handreck, 1965; Epstein, 1999; Carnelli et al., 2001; Casey et al., 2003). Si uptake is governed by active processes involving aquaporin transporter genes (Mitani and Ma, 2005; Ma and Yamaji, 2006; Ma et al., 2007; Yamaji

et al., 2008; Sparks et al., 2010). Si precipitation generally occurs at terminal sites of the transpiration stream in leaves and is affected by both the transpiration rate (Jones and Handreck, 1965) and the quantity of silicic acid in transpired water (Raven, 1983; Raven, 2003). Consequently, higher Si concentrations are oftentimes observed in leaves compared to other plant organs (Derry et al., 2005; Garvin, 2006; Blecker et al., 2007; Delvigne et al., 2009). Once deposited, phytoliths cannot be remobilized for translocation to other plant tissues (Raven, 1983). At the end of the growing season, phytoliths are recycled to soil reservoirs as single silicified cells and cell fragments through the decomposition of organic matter and plant death (Alexandre et al., 1997; Carnelli et al., 2001). Thereafter, they either dissolve or are preserved and buried in soil reservoirs from which Si can be taken up again by plants.

The present study uses a multi-tracer approach to examine sources and biogeochemical cycling of solutes in a temperate forested, shale catchment in central Pennsylvania. Specifically, a combination of  $^{87}\text{Sr}/^{86}\text{Sr}$ , Ca/Sr, and Ge/Si ratios in soil porewaters, exchangeable soils, leaves, sap waters, groundwaters, streamwaters, and drill core samples is analyzed. We take advantage of the well-documented SSHCZO where researchers have extensively characterized the catchment's geography (Lynch, 1976; West et al., 2011; Miller et al., 2013), geochemistry (Jin et al., 2010, 2011a,b, 2014; Jin and Brantley, 2011; Ma et al., 2010, 2011a,b, 2013, 2015; Brantley et al., 2013; Herndon et al., 2015), hydrology (Qu and Duffy, 2007; Lin and Zhou, 2008; Graham and Lin, 2011; Thomas et al., 2013), pedology (Lin, 2006; Lin et al., 2006; Lin and Zhou, 2008), and ecology (Wubbels, 2010; Naithani et al., 2013; Meinzer et al., 2013; Gaines et al., 2015).

## 2. Geological setting

Located in the ridge and valley region of central Pennsylvania, the Shale Hills Critical Zone Observatory (SSHCZO) encompasses a 7.9 ha temperate forested V-shaped first-order catchment (Fig. 1). The catchment lies within the Shavers Creek watershed of the Juniata River sub-basin and drains into the larger Susquehanna River. The stream channel is oriented in an east–west direction between narrow ridges (Jin et al., 2010). Mean annual precipitation is 1070 mm  $\text{yr}^{-1}$  and mean annual temperature is 10 °C (NOAA, 2007). Rainwater is relatively acidic (pH ~4.5) and enriched in nitrates and sulfates (NADP, 2013). Elevation varies from 310 m at the ridge top to 256 m at the stream outlet and slopes within the catchment range from 25 to 48% (Lin et al., 2006).

Four distinct landforms are present at the SSHCZO: a north (south-facing) slope, a south (north-facing) slope, a valley floor, and topographic depressional areas (swales). Deciduous forest and underbrush land cover dominates both the northern (south-facing) and southern (north-facing) slopes and the density of underbrush is higher on the south slope. Oak species (*Quercus* spp.) are prominent in deciduous land cover on the drier slope and ridge positions, with smaller populations of hickory (*Carya* spp.), pine (*Pinus* spp.), and maple (*Acer* spp.) also present. Western sides of the valley floor are comprised of Eastern hemlocks (*Tsuga canadensis*), while eastern sides consist of deciduous oak–hickory forest cover. Seven swales are dispersed throughout the catchment: five are located on the northern slope and two on the southern slope, with each divided by near-planar slopes. The current tree stand age is estimated to be between 70 and 80 years old with the most recent tree-harvesting event occurring in the 1930s (Wubbels, 2010).

At the SSHCZO, residual shale soils are present on the ridge tops and mid slope and valley floor soils are formed on a colluvial and alluvial mantle of shale chips (Jin and Brantley, 2011). These soils are underlain by the Silurian-age Rose Hill formation, an oxidized organic-poor marine shale with a few interbedded limestones (Lynch, 1976). The shale is comprised predominately of illite (58 wt.%), quartz (30 wt.%), vermiculitized chlorite (11 wt.%), and trace amounts of feldspar

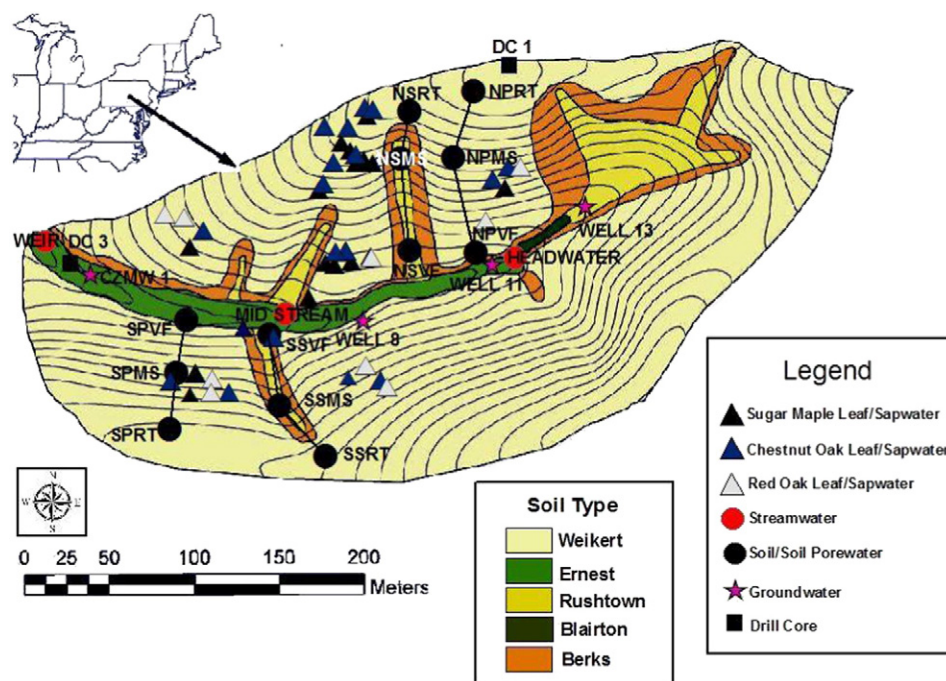


**Fig. 1.** Topographic map depicting sampling locations at the Susquehanna Shale Hills Critical Zone Observatory with contour lines shown in black (Figure modified from Thomas et al., 2013). Colors represent soil type based on field observations (Lin et al., 2006). Leaves and sap waters were collected throughout the observatory from three tree species: sugar maple (black triangles), chestnut oak (blue triangles), and red oak (gray triangles). Soils and soil porewaters (black circles) were sampled from the southern planar (SP) and south swale (SS) ridge top (RT), mid slope (MS), and valley floor (VF) locations. Drill core samples (black squares) were also collected from a northern ridge top borehole (DC 1) and from borehole CZMW 2 near the stream's weir (DC 3). Streamwaters (red circles) were sampled at the weir and at mid stream and headwater locations. Shallow (CZMW 1) and deep groundwaters (Wells 8, 11, and 13) (pink stars) were also collected. No spatial information was provided for a deep groundwater sample corresponding to sample ID CZMW 6 and, consequently, this sample is not displayed on the figure. Geospatial coordinate information can be found in Appendix A.

(plagioclase and K-feldspar), anatase ( $\text{TiO}_2$ ), Fe-oxides (magnetite and hematite), and zircon. Ankerite and pyrite are also present several meters below the surface at the northern ridge and at the valley floor near the stream's weir (Jin et al., 2010; Brantley et al., 2013). Shallow, well-drained soils at ridge locations (<50 cm) deepen downslope towards the stream (<300 cm). The convex-upward hillslope of the catchment consists of well-drained, oxic soils with a silty loam texture, while valley floor soils are characterized by redoximorphic features reflective of periodic reducing conditions from seasonal soil saturation (Lin et al., 2006). Throughout the SSHCZO, a 3 to 5 cm thick organic layer (Oe-horizon) is present consisting of decaying leaf litter and other organic materials. Effective rooting depth (i.e., depth to bedrock) ranges from 15 cm on ridge tops to 165 cm at selective slope locations.

High soil production rates at ridge locations ( $\sim 45 \text{ m My}^{-1}$ ) decrease exponentially downslope ( $\sim 15 \text{ m My}^{-1}$ ) (Ma et al., 2010). The average catchment-wide erosion rate is estimated to be  $15 \text{ m My}^{-1}$  based on cosmogenic  $^{10}\text{Be}$  dating of sediments (Jin et al., 2010). Further, regolith residence times range from 7 to 40 ky at the SSHCZO and increase from the ridge top to the valley floor (Ma et al., 2010). Swale and valley floor locations have been found to have residence times exceeding that of the last glacial maximum (ca. 15 kyra) (Gardner et al., 1991) and are hypothesized to have accumulated pre-glacial regolith (Ma et al., 2010). Jin et al. (2010, 2011a) and Brantley et al. (2013) predicted the order of mineral reaction fronts occurring at the SSHCZO. The first and deepest reaction front involves oxidative pyrite dissolution at approximately 23 and 9 m below the ground surface of the ridge and valley floor, respectively. Sulfuric acids generated by reactive pyrites and  $\text{CO}_2$  charged fluids in the unsaturated zone initiate carbonate dissolution at depths of 22 and 2 m at ridge and valley floor locations, respectively. A shallower reaction front follows involving plagioclase feldspar dissolution at 5 to 6 and 6 to 7 m below the ground surface of the ridge and valley floor, respectively. Above the feldspar reaction front and below the depth of augering refusal, clay weathering transforms primary illite

and chlorite minerals into secondary vermiculite and kaolinite resulting in a loss of soluble cations and fine particles. For planar hillslopes, chemical weathering rates are shown to decrease from ridge top to valley floor locations with elements such as Al and Si accumulating at the valley floor.

Numerous natural and anthropogenic perturbations have affected soil formation processes at the SSHCZO. Evidence of natural disturbance (e.g., freeze-thaw and stratified slope deposits) corresponds to a periglacial climate present in the region ca. 15 kya (Gardner et al., 1991). Anthropogenic disturbances at the SSHCZO include clear cutting of timber during colonial times and tree harvesting in the 1930s (Wubbels, 2010). Additionally, Herndon et al. (2011) identified remains of iron furnaces 20 miles from the catchment, a likely source of transported metals (e.g., Mn and Pb) to soils within the catchment via the atmospheric deposition of particulates. Similar to other locations in the northeastern United States, soils at the SSHCZO are affected by acid deposition with longer sulfur residence times in soils attributed to a combination of adsorption, precipitation, and mineralization processes (Jin et al., 2014).

### 3. Samples and methods

#### 3.1. Water sampling

Soil porewaters ( $n = 159$ ) were sampled from nested suction cup lysimeters installed at southern planar ridge top (SPRT), south swale ridge top (SSRT), southern planar mid slope (SPMS), south swale mid slope (SSMS), southern planar valley floor (SPVF), and south swale valley floor (SSVF) locations of the SSHCZO from May to July of 2013. SPRT and SSRT soil porewaters were sampled in 10 cm intervals at depths ranging from 10 to 30 cm. SPMS soil porewaters were sampled at depths of 10, 40, and 50 cm, while SSMS porewaters were sampled at depths ranging from 10 to 160 cm. SPVF and SSVF soil porewaters were

sampled in 10 cm depth intervals ranging from 20 to 60 cm and from 10 to 90 cm, respectively.

Streamwater grab samples were collected from weir, mid stream, and stream headwater locations in October of 2013. Groundwaters were also sampled at this time from boreholes at depths of 91 (CZMW 1) and 849 cm (CZMW 6) from the top of the casing to the water table and from wells at depths of 230 (Well 8), 478 (Well 11), and 276 cm (Well 13) from the top of the casing to the water table.

Xylem sap waters ( $n = 61$ ) were obtained from three tree species (*Acer saccharum*, ACSA—sugar maple; *Quercus prinus*, QUPR—chestnut oak; and *Quercus rubra*, QURU—red oak) representing 50% of all surveyed trees at the SSHCZO (Wubbels, 2010). Xylem sap water was extracted from sugar maple, chestnut oak, and red oak trees sampled at mid slope locations in northeastern, southeastern, northwestern, and southwestern quadrants of the catchment by means of a PMS pressure chamber.

Soil porewater, streamwater, groundwater, and sap water samples were filtered using 0.45  $\mu\text{m}$  Nylon syringe filters and acidified with a few drops of ultra pure concentrated nitric acid ( $\text{HNO}_3$ ). To digest dissolved organic matter, sap water was treated with hydrogen peroxide ( $\text{H}_2\text{O}_2$ , 30%) and gently heated. To improve signal to noise ratio on the mass spectrometer, filtered and acidified sample aliquots were concentrated by factors of 3 and 10 for Ge and Sr analyses, respectively, by evaporating sample volumes in an oven at 90 °C.

### 3.2. Exchangeable soil sampling

Soil samples ( $n = 19$ ) derived from ridge top (SPRT), mid slope (SPMS), and valley floor (SPVF) sites of the southern planar transect were hand augered until the point of refusal in October of 2011. Soil samples were collected from each horizon at all southern planar sites, sealed in Ziploc bags, and stored at field moisture conditions at 4 °C until analysis. Zero depth was defined as the bottom of the organic layer. Mid points of depth ranges were used to describe average soil characteristics for each horizon interval with soil samples collected from depths ranging from 0 to 21 cm, 0 to 33 cm, and 0 to 66 cm at SPRT, SPMS, and SPVF sites, respectively.

Exchangeable cations were extracted from soil samples using a method modified from Pett-Ridge et al. (2009). Approximately 10 g of air dried soil (<2 mm) were combined with 50 mL of 0.5 M ammonium acetate ( $\text{NH}_4\text{OAc}$ ). The resultant mixture was equilibrated for ~30 min on a shaker table and then centrifuged at 3000 rpm for ~10 min. Supernatant was collected and filtered using 0.45  $\mu\text{m}$  Nylon syringe filters.

### 3.3. Leaf sampling

Upper canopy leaves ( $n = 72$ ) were sampled from sugar maple, chestnut oak, and red oak trees at ridge top, mid slope, and valley floor sites in the northeastern quadrant of the catchment from June to September of 2011. Upper canopy leaves from the same three tree species were resampled monthly at mid slope positions in northeastern, southeastern, northwestern, and southwestern quadrants of the catchment from June to September of 2013. Leaves were obtained by rope climbing trees and using a pole cutter to remove a section of the tree branch. The leaves were subsequently placed in coin envelopes, transferred to the laboratory, and immediately dried at 60 °C to prevent decomposition.

Dried leaves were powdered using a coffee grinder. A leaf digestion method modified from Parr et al. (2001) was utilized where  $\text{HNO}_3$  (3 N) and  $\text{H}_2\text{O}_2$  (30%) were added in a 9:1 ratio to 0.5 g of powdered leaf weighed inside a Teflon reaction vessel. Vessels were left uncovered for approximately 10 min until bubbling from the reaction had ended and then recapped before being placed into the Milestone Ethos microwave digestion system. The digestion program was set to ramp the solution temperature to 180 °C within each vessel over a period of 5 min, remaining at this temperature for another ten minutes to

complete the digestion. After cooling to 21 °C, vessel contents were transferred into vials for future analyses. Samples were diluted by factors of 5 to 10 with  $\text{HNO}_3$  (2%) for analysis.

### 3.4. Drill core sampling

Rock chips and powders ( $n = 12$ ) were derived from a ridge top borehole in the northern quadrant of the catchment (DC 1) and from the CZMW 2 borehole near the stream's weir (DC 3) (Fig. 1.2) in May of 2014. Boreholes were drilled using a direct rotary air drill to depths of 25 m at DC 1 (Jin et al., 2010) and 16 m at DC 3 (Kuntz et al., 2011). Bulk samples consisting of rock fragments and granular powder were pulverized to pass through a 100 mesh sieve (<150  $\mu\text{m}$ ) and further ground to a fine powder using a mortar and pestle.

Carbonate and silicate fractions of borehole powders were extracted using a buffered ammonium acetate ( $\text{NH}_4\text{OAc}$ )/acetic acid ( $\text{HOAc}$ ) leach and a hydrofluoric acid ( $\text{HF}$ )/nitric acid ( $\text{HNO}_3$ ) digestion, respectively. Specifically, the carbonate fraction was extracted by combining 2.0 g of borehole powder with 20 mL of buffered  $\text{NH}_4\text{OAc}/\text{HOAc}$  solution. The resultant mixture was allowed to equilibrate overnight. To complete the dissolution, glacial acetic acid was added in 1 mL increments to each solution until bubbling from the reaction had ended. The resultant mixture was buffered to a pH between 4 and 5 with the  $\text{NH}_4\text{OAc}/\text{HOAc}$  solution, then equilibrated for approximately 5 min on a shaker table, and finally centrifuged at 3000 rpm for 20 min. Supernatant was collected and filtered using 0.45  $\mu\text{m}$  Nylon syringe filters. To remove colloidal material, 1 mL of  $\text{NH}_4\text{OAc}$  (0.5 M) was added to samples that were subsequently centrifuged at 3000 rpm for 20 min. Supernatant was then collected and filtered using 0.45  $\mu\text{m}$  Nylon syringe filters. Samples were dried completely and redissolved in  $\text{HNO}_3$  (2%) for major element and Sr isotope analyses. Following the  $\text{NH}_4\text{OAc}/\text{HOAc}$  leach, samples were dried in an oven at 130 °C and then ashed for 30 min at 600 °C in a muffle furnace to further oxidize any organic material. Subsamples ( $\approx 90$ –100 mg) were digested in a 3:1 ratio of concentrated HF to concentrated  $\text{HNO}_3$  with a few drops of perchloric acid ( $\text{HClO}_4$ ) added to remove any residual fluorides. The subsamples were dried completely and redissolved in  $\text{HNO}_3$  (2%) and hydrochloric acid ( $\text{HCl}$ , 2.5 N) for major element and Sr isotope analyses, respectively.

A lithium metaborate fusion procedure (Kurtz et al., 2002) was applied to DC 3 drill core samples collected at the CZMW 2 borehole near the stream's weir with Cody Shale (SCO-1) used as a reference standard for Ge analyses. Specifically, a 4:1 mixture of lithium metaborate flux ( $\text{LiBO}_2$ ) and sample were added to a graphite crucible that was heated in a muffle furnace set to 1050 °C for 15 min. Fused beads were added to 50 mL of  $\text{HNO}_3$  (10%) and then equilibrated on a shaker table to enhance dissolution of the fused bead. Filtered solutions (5 mL) were diluted using 35 mL of  $\text{HNO}_3$  (10%) for analysis.

### 3.5. Analytical techniques

Elemental concentrations were measured on a SPECTROBLUE inductively coupled plasma optical emission spectrometer (ICP-OES) with typical analytical uncertainties of 5% or less. To estimate analytical uncertainty on the ICP-OES, an internal standard solution of Sc, Y, In, and Yb, mixed in-line with sample before injection to the spray chamber and torch, was used as well as at least one check standard solution measured every 5 to 10 samples containing all of the analytes of interest in the same concentration range as the samples. Both solutions were prepared in-house from calibrated stock solutions (Spex Certiprep or iNorganic Ventures). For Sr isotope analyses, Sr separations were performed on sample aliquots using Eichrom Sr-Spec (waters, soils, leaves, and carbonate fraction of drill core) and AG-50-X8 (silicate fraction of drill core) resins with Sr isotope ratios measured on a VG Sector 54 thermal ionization mass spectrometer (TIMS). Sr isotopic compositions were corrected for mass fractionation using the exponential law where  $^{86}\text{Sr}/^{88}\text{Sr} = 0.1194$ . Analyses of NBS-987 standard yielded an

average  $^{87}\text{Sr}/^{86}\text{Sr} = 0.71023$ . The  $2\sigma$  uncertainties for the isotopic data based on repeat analyses of standards ranged between 0.00002 and 0.00005.

For Ge analysis, a  $^{70}\text{Ge}$  spike was added to each sample to obtain a  $^{70}\text{Ge}/^{74}\text{Ge}$  ratio of 3 or 4 depending on the Ge concentration estimated to be present based on the Si concentration of the sample. All samples were allowed to equilibrate with the  $^{70}\text{Ge}$  spike at room temperature for at least one night prior to analysis. Ge concentrations were measured on a Finnegan Element 2 inductively coupled mass spectrometer (ICP-MS), with typical relative standard deviations (RSDs) found to be between 3 and 5%. The continuous flow isotope-dilution hydride generation ICP-MS technique was used to measure Ge concentrations (Mortlock and Froelich, 1996; Kurtz, 2000). Samples, interspaced with Ge standards, check standards, and 2% nitric acid ( $\text{HNO}_3$ ) blanks, were placed into autosampler vials. From the vials, samples were pumped, individually, through a continuous flow apparatus. A 1 M Tris-HCl solution and 2% sodium borohydride solution ( $\text{NaBH}_4$ ) were pumped simultaneously through separate tubes. At the nexus of the three tubes, a reaction involving the sample and the Tris-HCl solution buffered the sample to a pH of 6. Simultaneously, a reaction involving the sample and sodium borohydride reduced the germanic acid to Ge hydride ( $\text{GeH}_4$ ). The  $\text{GeH}_4$  was stripped from solution through an inert argon (Ar) gas stream and passed through a Teflon filter membrane, at which point another Ar gas stream transferred it into the ICP torch, producing a Ge signal from which a  $^{70}\text{Ge}/^{74}\text{Ge}$  ratio was measured. A mass bias correction factor was applied to the  $^{70}\text{Ge}/^{74}\text{Ge}$  ratio measured for each sample using  $^{70}\text{Ge}/^{74}\text{Ge}$  ratios measured for standards and blanks within a run. Ge sample concentrations were calculated using the sample  $^{70}\text{Ge}/^{74}\text{Ge}$  ratio, the mass bias correction factor, and the masses of both sample and spike in the mixture. The quantity of Ge was determined using Eq. (1) below where  $Ab_s^{74}$  and  $Ab_n^{74}$  are the abundance of  $^{74}\text{Ge}$  in the spike (0.61%) and the natural abundance (36.54%), respectively,  $T$  is the moles of spike added,  $R_m$  and  $R_c$  are the mass bias and blank corrected  $^{70}\text{Ge}/^{74}\text{Ge}$  for the sample, respectively,  $R_s$  is the  $^{70}\text{Ge}/^{74}\text{Ge}$  in the spike (161.4), and  $R_n$  is the  $^{70}\text{Ge}/^{74}\text{Ge}$  natural abundance ratio (0.0562).

$$\text{Ge}(\text{mol}) = \left( \frac{Ab_s^{74}}{Ab_n^{74}} \right) \cdot T \cdot \frac{(R_m - R_s)}{(R_n - R_c)} \quad (1)$$

### 3.6. Data analysis methods

#### 3.6.1. Sr mixing calculations

Proportions of Sr derived from atmospheric and silicate mineral weathering end-members in ridge top and mid slope exchangeable soils and soil porewaters and leaves and sap waters are calculated using two-component mixing, where *atm*, *sil wea* and *carb wea* signify the atmospheric, silicate and carbonate weathering end-members, respectively (Eq. (2)).

$$X(\text{Sr})_{\text{atm}} = \frac{\left( \frac{^{87}\text{Sr}}{^{86}\text{Sr}} \right)_{\text{mix}} - \left( \frac{^{87}\text{Sr}}{^{86}\text{Sr}} \right)_{\text{sil wea}}}{\left( \frac{^{87}\text{Sr}}{^{86}\text{Sr}} \right)_{\text{atm}} - \left( \frac{^{87}\text{Sr}}{^{86}\text{Sr}} \right)_{\text{sil wea}}} \quad (2)$$

The carbonate weathering front beneath the ridge is hypothesized to begin at a depth of ~2200 cm (Jin et al., 2010; Jin et al., 2011a; Brantley et al., 2013). This depth lies well below those of deep southern planar and south swale ridge top exchangeable soils and soil porewaters (30 cm), deep southern planar mid slope exchangeable soils and soil porewaters (60 cm), and deep south swale mid slope soil porewaters (160 cm) sampled at the catchment. Consequently, effects of carbonate dissolution processes on Sr concentrations and Sr isotope compositions in ridge top and mid slope exchangeable soils and soil porewaters are

expected to be minimal and these reservoir components are modeled by two component mixing using atmospheric and silicate weathering end-members. Because plants are largely deriving solutes from the shallow soil exchange pool and soil porewater sources (Gaines et al., 2015, Tables 1, 2, 4 and 5, Fig. 2), the same end-members used to calculate atmospheric and weathering derived proportions of Sr in exchangeable soils and soil porewaters are incorporated into mixing calculations for leaves and sap waters.

The average  $^{87}\text{Sr}/^{86}\text{Sr}$  ratio for bulk precipitation at Penn State ( $^{87}\text{Sr}/^{86}\text{Sr} = 0.71054$ , Kim, 2007) was used as the atmospheric end-member. This value is similar to those reported by other researchers for precipitation in the northeastern United States (Dasch, 1969; Miller et al., 1993; Bailey et al., 1996; Dijkstra et al., 2003) where the

**Table 1**

$^{87}\text{Sr}/^{86}\text{Sr}$ , Ca/Sr and Ge/Si ratios for soil porewaters sampled from various depths at southern planar ridge top (SPRT), mid slope (SPMS), and valley floor (SPVF) sites and at south swale ridge top (SSRT), mid slope (SSMS), and valley floor (SSVF) locations.

Location	$^{87}\text{Sr}/^{86}\text{Sr}$	Ca/Sr (molar)	Ge/Si ( $\mu\text{mol}/\text{mol}$ )
<b>SPRT (n = 13)</b>			
10 cm	n.d. <sup>α</sup>	261	n.d. <sup>α</sup>
20 cm	0.72473	293 ± 9	3.4 ± 0.20
30 cm	0.72494	325 ± 12	2.9
Average	0.72484 ± 0.00011	300 ± 8	3.3 ± 0.18
Range	0.72473 to 0.72494	261 to 344	2.8 to 4.0
<b>SPMS (n = 18)</b>			
10 cm	0.72217	241 ± 8	2.0 ± 0.70
40 cm	0.72383 ± 0.00001	342 ± 10	1.1 ± 0.12
50 cm	0.72360 ± 0.00001	353 ± 11	1.8 ± 0.13
Average	0.72340 ± 0.00031	325 ± 12	1.7 ± 0.21
Range	0.72217 to 0.72384	221 to 383	0.9 to 3.3
<b>SPVF (n = 23)</b>			
20 cm	0.71865	341 ± 17	2.2 ± 0.04
30 cm	0.71854 ± 0.00001	340 ± 11	1.1 ± 0.30
40 cm	0.71827	334 ± 8	1.4 ± 0.04
50 cm	0.71818	227	1.5 ± 0.39
60 cm	0.71751 ± 0.00002	312 ± 9	1.2 ± 0.21
Average	0.71817 ± 0.00018	329 ± 7	1.6 ± 0.14
Range	0.71749 to 0.71865	227 to 400	0.8 to 2.4
<b>SSRT (n = 13)</b>			
10 cm	0.72400	195 ± 9	2.3 ± 0.38
20 cm	0.72648	131 ± 13	2.3 ± 0.23
30 cm	0.72480	231 ± 13	2.3 ± 0.17
Average	0.72509 ± 0.00073	184 ± 13	2.3 ± 0.18
Range	0.72400 to 0.72648	113 to 244	1.2 to 3.4
<b>SSMS (n = 60)</b>			
10 cm	n.d. <sup>α</sup>	324	2.3
20 cm	0.72422	232 ± 14	1.7 ± 0.18
40 cm	0.72434 ± 0.00023	211 ± 7	1.8 ± 0.06
60 cm	0.72531	218 ± 11	1.5 ± 0.12
80 cm	0.72531	238 ± 9	1.4 ± 0.17
100 cm	0.72586 ± 0.00004	260 ± 5	0.9 ± 0.05
120 cm	0.72590 ± 0.00010	260 ± 6	1.0 ± 0.02
140 cm	0.72575 ± 0.00003	257 ± 5	0.9 ± 0.04
160 cm	0.72586 ± 0.00007	258 ± 8	0.9 ± 0.03
Average	0.72546 ± 0.00016	246 ± 4	1.2 ± 0.07
Range	0.72411 to 0.72599	181 to 324	0.7 to 2.3
<b>SSVF (n = 32)</b>			
10 cm	0.71895 ± 0.00005	425 ± 14	1.4 ± 0.68
20 cm	0.71997	325 ± 15	1.9 ± 0.13
30 cm	0.71934	248 ± 10	2.0 ± 0.03
40 cm	0.71970 ± 0.00002	230 ± 12	1.1 ± 0.12
50 cm	n.d. <sup>α</sup>	244 ± 5	1.1 ± 0.12
60 cm	n.d. <sup>α</sup>	255 ± 14	1.2 ± 0.20
70 cm	n.d. <sup>α</sup>	168	1.4
80 cm	0.72005	168 ± 3	0.7 ± 0.19
90 cm	n.d. <sup>α</sup>	237	n.d. <sup>α</sup>
Average	0.71952 ± 0.00017	273 ± 15	1.4 ± 0.13
Range	0.71889 to 0.72005	162 to 456	0.5 to 2.8

<sup>α</sup> The 'n.d.' term refers to a sample where a measurement was not determined.

**Table 2**

$^{87}\text{Sr}/^{86}\text{Sr}$  and Ca/Sr ratios for exchangeable soils sampled from various depths at southern planar ridge top (SPRT), mid slope (SPMS), and valley floor (SPVF) locations.

Location	$^{87}\text{Sr}/^{86}\text{Sr}$	Ca/Sr (molar)
<i>SPRT (n = 3)</i>		
0 cm	0.72322	224
13.5 cm	0.72276	242
18.5 cm	0.72385	174
<i>Depth Weighted Mean</i>	$0.72329 \pm 0.00032$	$216 \pm 20$
<i>Range</i>	0.72276 to 0.72385	174 to 224
<i>SPMS (n = 5)</i>		
6.5 cm	0.72118	152
17.0 cm	0.72317	100
24.0 cm	0.72443	134
29.5 cm	0.72472	134
32.5 cm	0.72493	134
<i>Depth Weighted Mean</i>	$0.72329 \pm 0.00032$	$216 \pm 20$
<i>Range</i>	0.72118 to 0.72493	100 to 152
<i>SPVF (n = 11)</i>		
3.0 cm	0.71780	214
10.0 cm	0.71834	176
18.0 cm	0.71877	150
25.0 cm	0.71890	154
32.0 cm	0.71899	152
39.0 cm	0.71939	140
44.0 cm	0.71954	144
49.5 cm	0.71944	150
56.0 cm	0.71933	156
61.0 cm	0.71921	132
64.0 cm	0.71892	106
<i>Depth Weighted Mean</i>	$0.71892 \pm 0.00016$	$155 \pm 8$
<i>Range</i>	0.71780 to 0.71954	106 to 214

Sr isotope composition in precipitation has been shown to be relatively uniform over time.

Traditionally, the weathering end-member is defined by the Sr isotope composition of minerals in rocks and soils, with each mineral displaying a distinctive weathering rate and  $^{87}\text{Sr}/^{86}\text{Sr}$  ratio. Spatial variability in the mineralogical composition of the weathered substrate and temporal variability in the weathering rates of individual minerals both directly affect the Sr isotope composition in exchangeable soils and soil porewaters. In this study, the fine-grained nature of shales and soils at the catchment preclude identification of Sr isotope compositions for mineral separates in rocks and soils. Instead, the average  $^{87}\text{Sr}/^{86}\text{Sr}$  ratio for ‘weathered’ shale ( $^{87}\text{Sr}/^{86}\text{Sr} = 0.72967$ , Table 8) was used as the silicate weathering end-member. This value is taken as the average value from the  $\text{NH}_4\text{OAc}/\text{HOAc}$  leach on ‘carbonate free’ DC 1 drill core samples (DC 1–21 to DC 1–36, Table 8). Although the DC 1 drill core is not immediately adjacent to the exchangeable soil and soil porewater sites sampled in the southern quadrant of the catchment (Fig. 1), Jin et al. (2010) found that average compositions and densities of deep soils derived from soil cores across the catchment are similar to those of DC 1 drill core samples. Based on these observations, use of ‘carbonate free’ DC 1 drill core  $^{87}\text{Sr}/^{86}\text{Sr}$  ratios for determination of the ‘weathered’ shale end-member value seems reasonable. Given the range of  $^{87}\text{Sr}/^{86}\text{Sr}$  ratios measured for southern planar ridge top and mid slope samples and south swale ridge top and mid slope samples (Tables 1 and 2), the  $^{87}\text{Sr}/^{86}\text{Sr}$  ratio of ‘weathered’ shale ( $^{87}\text{Sr}/^{86}\text{Sr} = 0.72967$ , Table 8) was used as the more appropriate choice for the silicate weathering end-member. Lending support for use of ‘weathered’ shale as the silicate weathering end-member are mineralogical observations of high chemical weathering rates as calculated based on average soil chemistry, soil density, and soil thickness and low cation exchange capacities relative to unweathered parent drill core samples for ridge top and mid slope exchangeable soils and soil porewaters (Jin et al., 2010).

Lower  $^{87}\text{Sr}/^{86}\text{Sr}$  ratios in valley floor exchangeable soils and soil porewaters (Tables 1 and 2) and streamwaters and groundwaters (Table 7) compared to ridge top and mid slope exchangeable soils and soil porewaters (Tables 1 and 2) imply that a source less radiogenic

than shale is affecting their Sr concentrations and Sr isotope compositions. Further, relatively alkaline streamwaters and groundwaters with high Ca and Mg concentrations (Table 7, Jin et al., 2011b) are consistent with carbonate dissolution. At the nearby DC-3 core, carbonates were identified at the 200 m depth (Jin et al., 2010; Brantley et al., 2013). We take the average  $^{87}\text{Sr}/^{86}\text{Sr}$  ratio for the carbonate fraction of DC 3 drill core samples ( $^{87}\text{Sr}/^{86}\text{Sr} = 0.71132$ , Table 8) as the carbonate mineral weathering end-member here. We infer that the shallow carbonates as found in the DC-3 core are influencing Sr concentrations and  $^{87}\text{Sr}/^{86}\text{Sr}$  ratios of valley floor exchangeable soils and soil porewaters and streamwaters and groundwaters (depth range: 90 to 850 cm).

The average  $^{87}\text{Sr}/^{86}\text{Sr}$  ratio for the silicate fraction of DC 1 and DC 3 drill core samples (i.e., unweathered shale end-member,  $^{87}\text{Sr}/^{86}\text{Sr} = 0.74558$ , Table 8) is selected as the silicate mineral weathering end-member for valley floor exchangeable soils and soil porewaters and streamwaters and groundwaters. Using average soil chemistry, soil density, and soil thickness, Jin et al. (2010) demonstrated that chemical weathering processes are slow at valley floor sites. Additionally, C.E.C.s of valley floor soils are comparable to parent materials suggesting that illite and chlorite dissolution processes are insignificant at valley floor sites of the catchment (Jin et al., 2010). As shown in Table 8, ranges of  $^{87}\text{Sr}/^{86}\text{Sr}$  ratios in residual material are relatively uniform between DC 1 ridge top and DC 3 valley floor drill core sites. Thus, a composite average  $^{87}\text{Sr}/^{86}\text{Sr}$  ratio using data compiled from both sites for determination of the silicate weathering end-member seems appropriate.

Proportions of Sr derived from carbonate and silicate mineral weathering end-members are determined using two-component mixing on Cl normalized Sr isotope ratios ( $^{87}\text{Sr}/^{86}\text{Sr}^*$ ). In this way, the mass fraction of Sr derived from the atmosphere ( $X(\text{Sr})_{\text{atm}}$ ) is corrected for enabling calculation of relative proportions of Sr derived from carbonate and silicate mineral weathering sources using two-component mixing. Calculation of  $^{87}\text{Sr}/^{86}\text{Sr}^*$  is done by first normalizing Sr elemental concentrations ( $[\text{Sr}]^*$ ) using Sr and Cl concentrations measured in precipitation (*atm*) and in the sample (*mix*) (Eq. (3)):

$$[\text{Sr}]_{\text{mix}}^* = [\text{Sr}]_{\text{mix}} - \left(\frac{\text{Sr}}{\text{Cl}}\right)_{\text{atm}} \cdot [\text{Cl}]_{\text{mix}} \quad (3)$$

Sr isotope ratios corrected for atmospheric inputs ( $^{87}\text{Sr}/^{86}\text{Sr}^*$ ) are then given by Eq. (4):

$$\left(\frac{^{87}\text{Sr}}{^{86}\text{Sr}}\right)_{\text{mix}}^* = \frac{\left(\frac{^{87}\text{Sr}}{^{86}\text{Sr}}\right)_{\text{mix}} - \left[X(\text{Sr})_{\text{atm}} \cdot \left(\frac{^{87}\text{Sr}}{^{86}\text{Sr}}\right)_{\text{atm}}\right]}{[\text{Sr}]_{\text{mix}}^* / [\text{Sr}]_{\text{atm}}^*} \quad (4)$$

Cl normalized Sr isotope ratios ( $^{87}\text{Sr}/^{86}\text{Sr}^*$ ) are used to constrain proportions of Sr derived from carbonate (*carb wea*) and silicate (*sil wea*) weathering as shown below in Eq. (5):

$$X(\text{Sr})_{\text{carb wea}} = \frac{\left(\frac{^{87}\text{Sr}}{^{86}\text{Sr}}\right)_{\text{mix}}^* - \left(\frac{^{87}\text{Sr}}{^{86}\text{Sr}}\right)_{\text{sil wea}}}{\left(\frac{^{87}\text{Sr}}{^{86}\text{Sr}}\right)_{\text{carb wea}} - \left(\frac{^{87}\text{Sr}}{^{86}\text{Sr}}\right)_{\text{sil wea}}} \quad (5)$$

### 3.6.2. Streamwater flux and carbonate propagation front calculations

Using elemental and stream discharge data compiled from 2008 to 2010 (Brantley and Duffy, 2008, 2009, 2010 and Duffy, 2008, 2009, 2010), Sr fluxes ( $\text{mol ha}^{-1} \text{y}^{-1}$ ) are determined by dividing the product of the geometric mean of Sr concentration and stream discharge at a given position (stream headwater, mid stream, weir) by the total watershed area of the catchment. Fluxes are apportioned into atmospheric and weathering sources using Eqs. (2) and (5). Ca fluxes ( $\text{mol ha}^{-1} \text{y}^{-1}$ ) are determined using average molar Ca/Sr ratios and previously calculated Sr flux values. In order to determine the atmospheric Ca flux, the average molar Ca/Sr ratio of bulk precipitation at Penn State

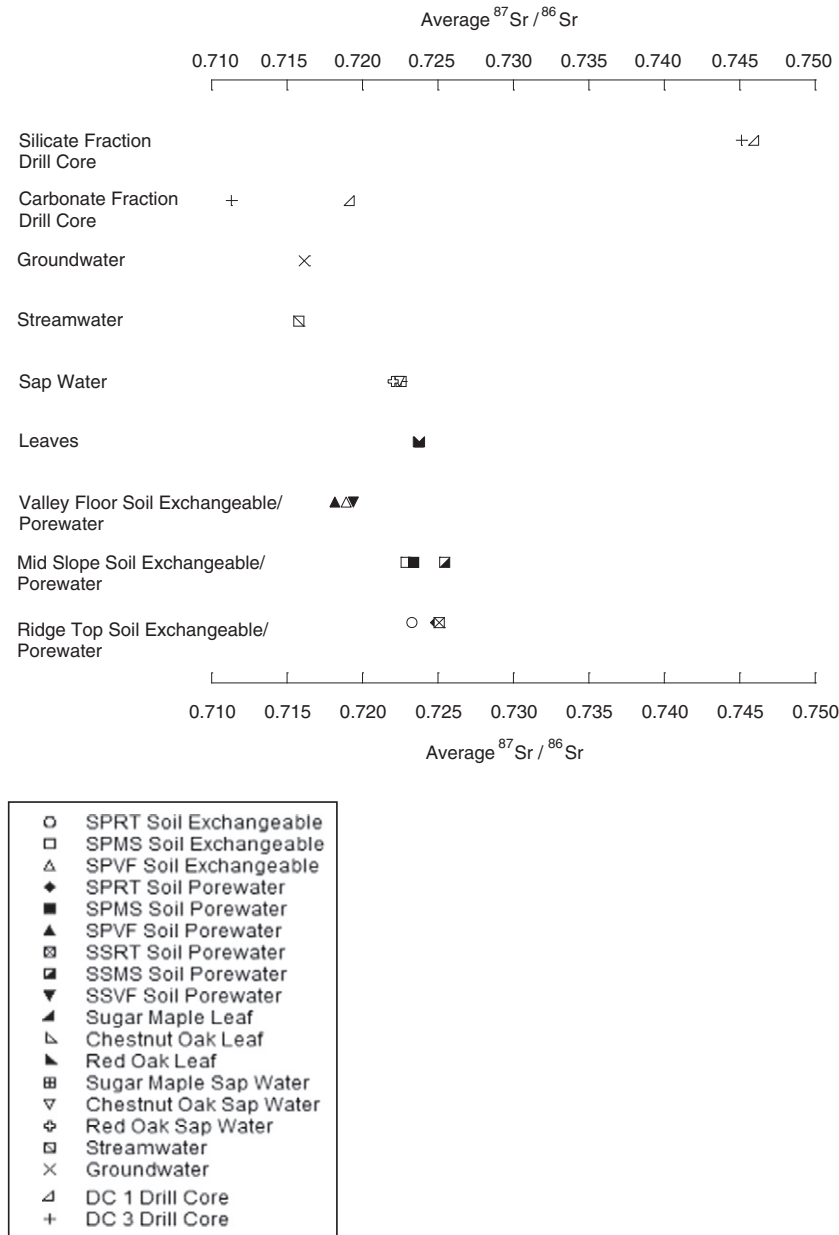


**Fig. 2.** Average  $^{87}\text{Sr}/^{86}\text{Sr}$  ratios for southern planar ridge top, mid slope, and valley floor exchangeable soils and soil porewaters, south swale ridge top, mid slope, and valley floor soil porewaters, sugar maple, chestnut oak, and red oak leaves and sap water, streamwaters and groundwaters, and carbonate and silicate fractions of DC 1 and DC 3 drill core samples. Note: For carbonate fractions, average  $^{87}\text{Sr}/^{86}\text{Sr}$  ratios only include samples where carbonates were observed in the quantitative mineralogy (Jin et al., 2010, Brantley et al., 2013).

( $\text{Ca}/\text{Sr} = 233 \pm 6$ , NADP, 2013) is multiplied by the atmospheric Sr flux at a given streamwater position (stream headwater, mid stream, weir). For weathering derived Ca fluxes, the atmospheric Sr flux is first subtracted from the total Sr flux. This value is then multiplied by the average molar Ca/Sr ratio of the carbonate end-member ( $\text{Ca}/\text{Sr} = 882$ ). Proportions of Ca derived from carbonate (*carb wea*) and silicate (*sil wea*) mineral weathering end-members in streamwaters are determined using two-component mixing (Eq. (6)) on Cl normalized Sr isotope ratios ( $(^{87}\text{Sr}/^{86}\text{Sr})^*$ ), where SW represents streamwater.

$$X(\text{Ca})_{\text{carb wea}} = \frac{\left[ \left( \frac{^{87}\text{Sr}}{^{86}\text{Sr}} \right)_{\text{SW}}^* - \left( \frac{^{87}\text{Sr}}{^{86}\text{Sr}} \right)_{\text{sil wea}} \right] \cdot \left( \frac{\text{Sr}}{\text{Ca}} \right)_{\text{sil wea}}}{\left[ \left( \frac{^{87}\text{Sr}}{^{86}\text{Sr}} \right)_{\text{SW}}^* - \left( \frac{^{87}\text{Sr}}{^{86}\text{Sr}} \right)_{\text{sil wea}} \right] \cdot \left( \frac{\text{Sr}}{\text{Ca}} \right)_{\text{sil wea}} + \left[ \left( \frac{^{87}\text{Sr}}{^{86}\text{Sr}} \right)_{\text{carb wea}} - \left( \frac{^{87}\text{Sr}}{^{86}\text{Sr}} \right)_{\text{SW}}^* \right] \cdot \left( \frac{\text{Sr}}{\text{Ca}} \right)_{\text{carb wea}}} \quad (6)$$

To calculate the rate of propagation of the carbonate weathering front, calcite, as opposed to ankerite, is chosen to represent the carbonate source at the DC 3 valley floor site. Brantley et al. (2013) observed precipitation of secondary calcites at depths below the carbonate weathering front (~4 m depth) at the valley floor. Carbonate fractions of DC1–37 and DC1–38 samples at the ridge displayed much higher  $^{87}\text{Sr}/^{86}\text{Sr}$  ratios (0.71935 and 0.71910, respectively, Table 8) than those observed for DC 3 drill core samples at the valley floor (average  $^{87}\text{Sr}/^{86}\text{Sr} = 0.71132$ ). The Sr isotope data indicate that the ankerite in the deep DC 1 core and the calcite sampled in the DC 3 core represent two different and unrelated generations of carbonate.

### 3.6.3. Plant fractionation factors

Fractionation factors ( $K_{\text{Sr}/\text{Ca}}$  and  $K_{\text{Ge}/\text{Si}}$ ) are calculated for sugar maple, chestnut oak, and red oak species in southwestern and southeastern quadrants by dividing the trace element ratio (e.g., Sr/Ca or

Ge/Si) in leaves to the corresponding ratio in the soil porewater (PW) solution as shown below in Eq. (7):

$$K_{trace/major} = \frac{\left[ \frac{trace}{major} \right]_{leaf}}{\left[ \frac{trace}{major} \right]_{PW}} \quad (7)$$

Fractionation factors less than one reflect discrimination against the trace element (e.g., Sr or Ge). In the case of preferential discrimination against the trace element, the upper and lower bounds are defined as no discrimination ( $K = 1$ ) between the major and trace element and the complete exclusion of the trace element ( $K = 0$ ) by vegetation, respectively. Considering soil porewater is the most readily available

reservoir of plant nutrients (Wyttenbach et al., 1995), trace element ratios of soil porewaters are used in the calculation.

#### 4. Results

##### 4.1. Soil porewaters and exchangeable soils

Sr isotope, Ca/Sr, and Ge/Si ratios for soil porewaters sampled at various depths from southern planar and south swale sites are reported in Table 1, while Sr isotope and Ca/Sr ratios for southern planar exchangeable soils are shown in Table 2. Average Sr isotope, Ca/Sr, and Ge/Si ratios are also presented in Figs. 2 to 4, respectively, while Sr isotope, Ca/Sr, and Ge/Si ratios are displayed as functions of depth in Figs. 5 to 7, respectively. Monthly average Ca/Sr and Ge/Si ratios for soil porewaters

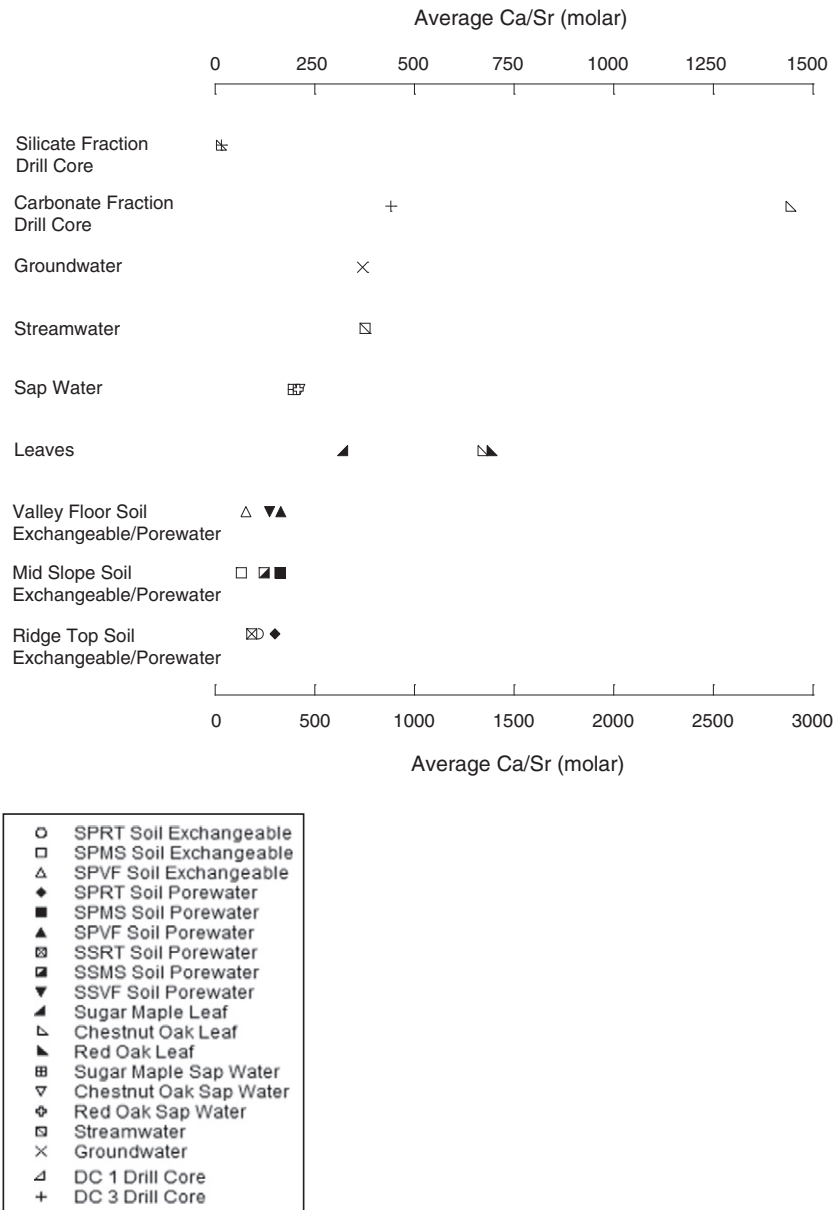


**Fig. 3.** Average Ca/Sr ratios for southern planar ridge top, mid slope, and valley floor exchangeable soils and soil porewaters, south swale ridge top, mid slope, and valley floor soil porewaters, sugar maple, chestnut oak, and red oak leaves and sap water, streamwaters and groundwaters, and carbonate and silicate fractions of DC 1 and DC 3 drill core samples. Note: For carbonate fractions, average Ca/Sr ratios only include samples where carbonates were observed in the quantitative mineralogy (Jin et al., 2010, Brantley et al., 2013). Additionally, average Ca/Sr ratios for silicate fractions are derived from “carbonate free” samples or samples where carbonate contamination is unlikely.

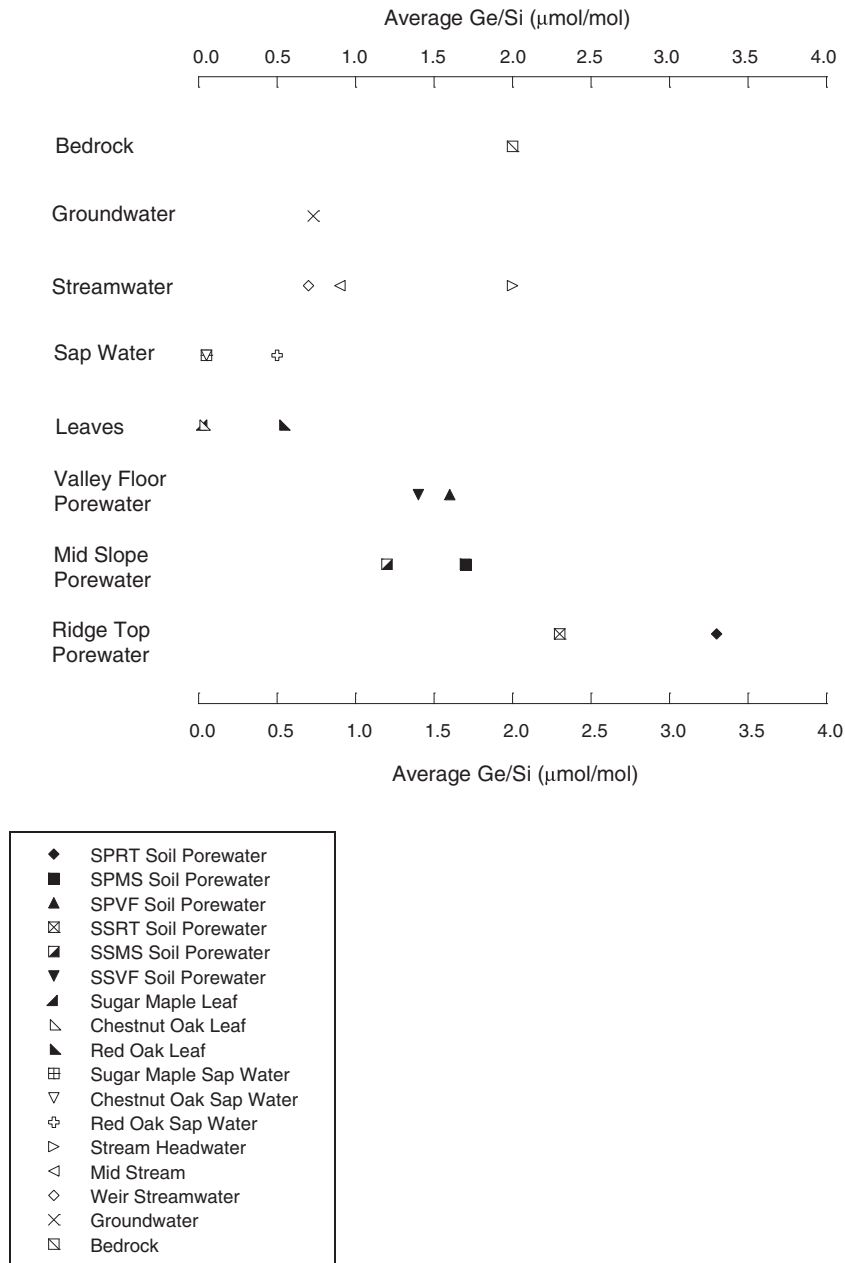


**Fig. 4.** Average Ge/Si ratios for southern planar and south swale ridge top, mid slope, and valley floor soil porewaters, sugar maple, chestnut oak, and red oak leaves and sap waters, and streamwaters, groundwaters, and bedrock. Note: The average Ge/Si ratio for DC 3 drill core samples is shown.

sampled at various transect locations over the course of the growing season are listed in Table 3.

#### 4.2. Leaves and sapwaters

Sr isotope, Ca/Sr, and Ge/Si ratios for sugar maple, chestnut oak, and red oak leaves and sap waters sampled from mid slope positions at northeastern, northwestern, southeastern, and southwestern quadrants of the catchment are reported in Tables 4 and 5 and displayed in Figs. 2 through 4. Monthly average leaf Ca and Si concentrations are listed in Table 6 and shown in Fig. 8.

#### 4.3. Groundwaters and streamwaters

Sr, Ca, Cl, Si, and Ge concentrations, pH values, and Ca/Sr,  $^{87}\text{Sr}/^{86}\text{Sr}$ ,  $(^{87}\text{Sr}/^{86}\text{Sr})^*$ , and Ge/Si ratios for groundwaters and streamwaters sampled at the catchment are reported in Table 7. Average Sr isotope, Ca/Sr, and Ge/Si ratios are also shown in Figs. 2 through 4.

#### 4.4. Drill core

$^{87}\text{Sr}/^{86}\text{Sr}$ , Ca/Sr, and Ge/Si ratios for drill cores sampled at the ridge top borehole (DC 1) and at the CZMW 2 borehole near the stream's

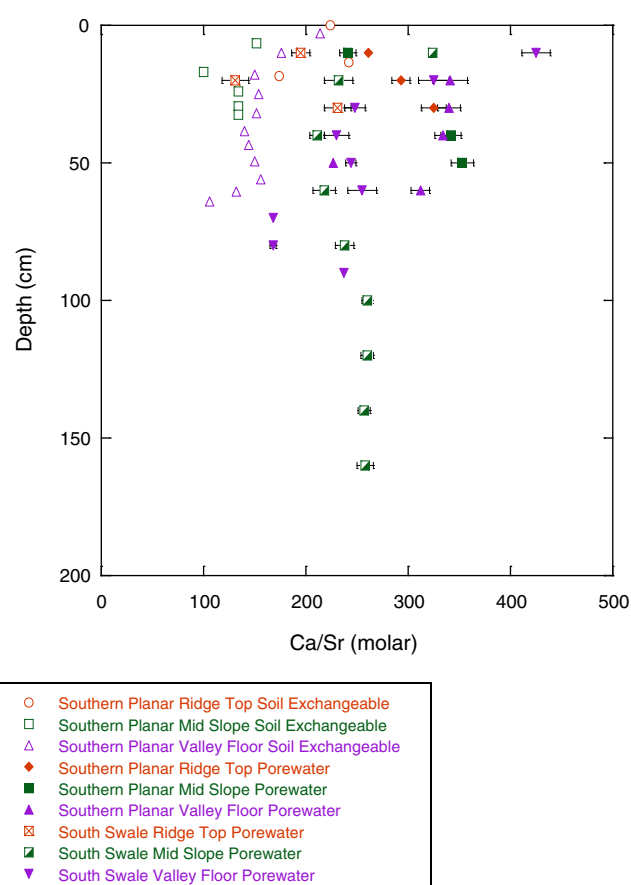
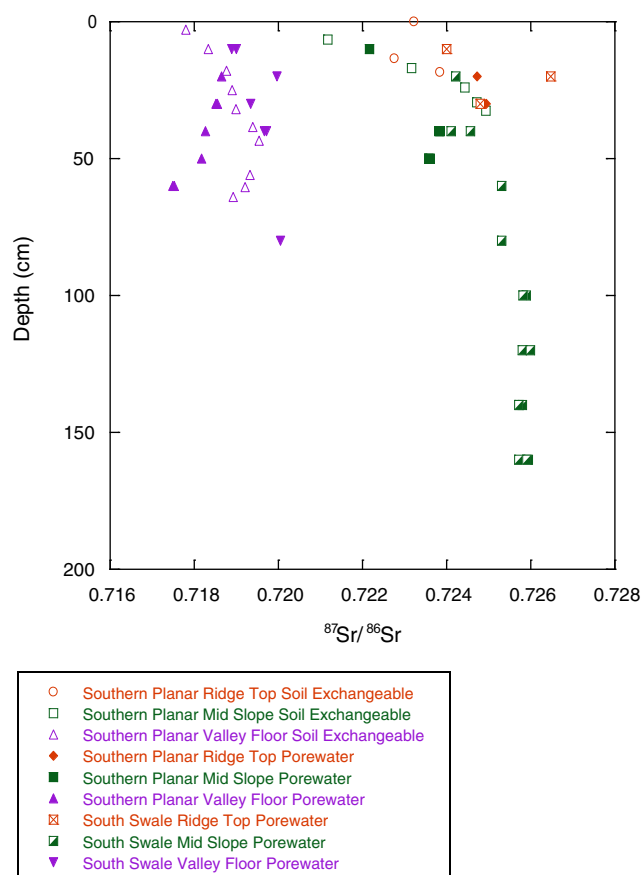


**Fig. 5.** Depth versus  $^{87}\text{Sr}/^{86}\text{Sr}$  ratio for southern planar ridge top (orange), mid slope (green), and valley floor (purple) exchangeable soils and soil porewaters and for south swale ridge top (orange), mid slope (green), and valley floor (purple) soil porewaters.

**Fig. 6.** Depth versus Ca/Sr ratio for southern planar ridge top (orange), mid slope (green), and valley floor (purple) exchangeable soils and soil porewaters and for south swale ridge top (orange), mid slope (green), and valley floor (purple) soil porewaters.

weir (DC 3) are reported in Table 8. Average Sr isotope, Ca/Sr, and Ge/Si ratios are also shown in Figs. 2 through 4.

## 5. Discussion

### 5.1. Spatiotemporal patterns in soil and water chemistry

#### 5.1.1. Exchangeable soils and soil porewaters

Site specific differences in Sr isotope ratio (Tables 1 and 2, Fig. 2) are quite pronounced, with downslope (i.e., valley floor) exchangeable soil and soil porewater  $^{87}\text{Sr}/^{86}\text{Sr}$  ratios observed to be significantly lower than those for exchangeable soils and soil porewaters sampled at upslope (i.e., ridge top and mid slope) locations. This agrees with field and geochemical observations by Lin (2006) and Jin et al. (2011b) that suggest recharge of carbonate affected groundwaters to valley floor soils and soil porewaters at the catchment. However, Ca/Sr ratios of exchangeable soils and soil porewaters (Fig. 3) are relatively uniform irrespective of sampling site. In fact, Ca/Sr ratios in swale porewaters are moderately lower than those observed in planar porewaters. Swale soils are known to be wetter than planar soils and hydrologically connected to the stream even during dry periods (Lin et al., 2006; Qu and Duffy, 2007; Takagi and Lin, 2012). Further, Andrews et al. (2011) found higher dissolved organic carbon concentrations in the uppermost soil horizons at swale ( $\text{DOC} > 1 \text{ mM}$ ) relative to planar ( $\text{DOC} < 1 \text{ mM}$ ) locations consistent with the accumulation of soil organic matter in geomorphological depressions of swales. During rain events, dissolved organic carbon loss from swale soils to the stream will be accompanied by loss of biologically cycled elements closely associated with soil

organic matter (e.g., Ca). Hence, the lower Ca/Sr ratios observed in swale compared to planar porewaters. For Ge/Si ratios, ridge top soil porewaters have significantly higher ratios (Tables 1 and 2, Fig. 4) compared to downslope (i.e., mid slope and valley floor) soil porewaters. Mean fractionation factors calculated for sugar maple ( $K_{\text{Ge/Si}} = 0.01$ ), chestnut oak ( $K_{\text{Ge/Si}} = 0.01$ ), and red oak ( $K_{\text{Ge/Si}} = 0.27$ ) species lend support to the preferential discrimination against Ge relative to Si by plants at the catchment. Effects of plant activities at the surface responsible for leaching Ge to soil porewaters are expected to be more pronounced at shallow ridge top sites (30 cm deep) compared to deeper mid slope (50 and 160 cm deep) and valley floor (60 and 90 cm deep) sites. On the other hand, Ge/Si ratios in porewaters sampled from mid slope and valley floor sites have more substantial mineral horizons (i.e., A, B, and C horizons) and should reflect primary weathering processes which partition Ge into secondary aluminosilicates.

Within sites, Sr isotope ratios for exchangeable soils and soil porewaters are relatively uniform as a function of depth and fall within a narrow range of values (Tables 1 and 2, Fig. 5). For upslope sites unaffected by carbonates,  $^{87}\text{Sr}/^{86}\text{Sr}$  ratios of exchangeable soil horizons and soil porewaters are observed to be in close agreement to those found for leaves and sap waters (Tables 1, 2, 4, and 5, Fig. 2). This suggests that biological nutrient cycling processes at the catchment are rapidly homogenizing Sr inputs added from weathering and atmospheric sources, particularly for exchangeable soils and soil porewaters sampled at shallow depths. Results from end-member mixing calculations (Eq. (2)) indicate that proportions of atmospherically derived Sr in southeastern and southwestern leaves and sap waters sampled at mid slope positions

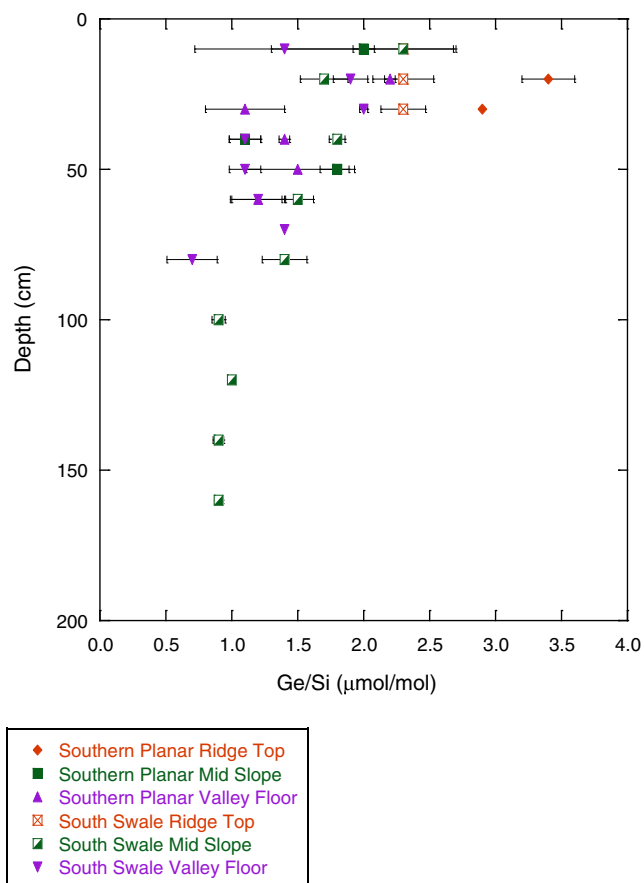


Fig. 7. Depth versus Ge/Si ratio for southern planar and south swale ridge top (orange), mid slope (green), and valley floor (purple) soil porewaters.

correspond to those reported for organic soil horizons and shallow soil porewaters sampled from similar quadrants and transect positions. Accordingly, lower  $^{87}\text{Sr}/^{86}\text{Sr}$  ratios and higher atmospheric proportions of Sr are also observed for shallow southern planar mid slope (southwestern) soil porewaters compared to those sampled at the south swale (southeastern) mid slope location. Proportions of Sr derived from atmospheric sources in southwestern sugar maple, chestnut oak, and red oak leaves and sap waters are 0.40, 0.43; and 0.47, respectively, compared to 0.33, 0.38, and 0.33, for leaves and sap waters collected from corresponding species in the southeastern quadrant. Additionally, minimal variation in leaf and sap water  $^{87}\text{Sr}/^{86}\text{Sr}$  ratio observed between species sampled from similar quadrants and transect positions imply similar sources (i.e., shallow exchangeable and porewater pools) from which plants are acquiring Sr (and by inference, Ca). This complements  $\delta^{18}\text{O}$  studies by Gaines et al. (2015) that show leaf and sap water values to correspond more closely to shallow underlying soils than to groundwaters.

Table 3

Seasonal Ca/Sr ratios for soil porewaters sampled from southern planar and south swale ridge top, mid slope, and valley floor locations.

Transect location	May		June		July	
	Ca/Sr (molar)	Ge/Si ( $\mu\text{mol}/\text{mol}$ )	Ca/Sr (molar)	Ge/Si ( $\mu\text{mol}/\text{mol}$ )	Ca/Sr (molar)	Ge/Si ( $\mu\text{mol}/\text{mol}$ )
Southern Planar Ridge Top (n = 13)	323 $\pm$ 13	2.9 $\pm$ 0.05	302 $\pm$ 12	3.4 $\pm$ 0.08	280 $\pm$ 14	3.6 $\pm$ 0.40
Southern Planar Mid Slope (n = 18)	360 $\pm$ 17	1.3 $\pm$ 0.20	310 $\pm$ 16	1.6 $\pm$ 0.16	294 $\pm$ 24	2.7 $\pm$ 0.54
Southern Planar Valley Floor (n = 23)	351 $\pm$ 7	1.4 $\pm$ 0.23	294 $\pm$ 15	1.6 $\pm$ 0.17	317 $\pm$ 8	1.9 $\pm$ 0.25
South Swale Ridge Top (n = 13)	219 $\pm$ 13	1.8	174 $\pm$ 17	2.3 $\pm$ 0.26	167 $\pm$ 30	2.6 $\pm$ 0.10
South Swale Mid Slope (n = 60)	258 $\pm$ 6	1.0 $\pm$ 0.13	247 $\pm$ 6	1.2 $\pm$ 0.10	231 $\pm$ 6	1.2 $\pm$ 0.12
South Swale Valley Floor (n = 32)	260 $\pm$ 30	1.9	265 $\pm$ 24	1.2 $\pm$ 0.13	291 $\pm$ 27	1.8 $\pm$ 0.29

Table 4

$^{87}\text{Sr}/^{86}\text{Sr}$ , Ca/Sr, and Ge/Si ratios for sugar maple, chestnut oak, and red oak leaves sampled at mid slope positions in various quadrants of the catchment.

Tree species	$^{87}\text{Sr}/^{86}\text{Sr}$	Ca/Sr (molar)	Ge/Si ( $\mu\text{mol}/\text{mol}$ )
<i>Northeastern</i>			
Sugar Maple (n = 4)	0.72411 $\pm$ 0.00017	595 $\pm$ 10	0.03 $\pm$ 0.005
Chestnut Oak (n = 6)	0.72382 $\pm$ 0.00019	1181 $\pm$ 41	0.03 $\pm$ 0.003
Red Oak (n = 7)	0.72275	1128 $\pm$ 19	0.56 $\pm$ 0.058
<i>Northwestern</i>			
Sugar Maple (n = 6)	0.72221 $\pm$ 0.00003	730 $\pm$ 17	0.05 $\pm$ 0.007
Chestnut Oak (n = 4)	n.d. <sup>a</sup>	1588 $\pm$ 71	0.04 $\pm$ 0.006
Red Oak (n = 6)	n.d. <sup>a</sup>	1645 $\pm$ 38	0.69 $\pm$ 0.026
<i>Southeastern</i>			
Sugar Maple (n = 6)	0.72341	582 $\pm$ 23	0.03 $\pm$ 0.006
Chestnut Oak (n = 8)	0.72235	1290 $\pm$ 50	0.02 $\pm$ 0.003
Red Oak (n = 6)	0.72409 $\pm$ 0.00019	1294 $\pm$ 92	0.49 $\pm$ 0.048
<i>Southwestern</i>			
Sugar Maple (n = 6)	0.72258	671 $\pm$ 22	0.02 $\pm$ 0.007
Chestnut Oak (n = 7)	0.72101	1373 $\pm$ 42	0.02 $\pm$ 0.002
Red Oak (n = 7)	n.d. <sup>a</sup>	1449 $\pm$ 56	0.56 $\pm$ 0.068
<i>All locations</i>			
Average Sugar Maple (n = 22)	0.72388 $\pm$ 0.00019	649 $\pm$ 16	0.03 $\pm$ 0.004
Range Sugar Maple	0.72218 to 0.72585	534 to 796	0.06 to 0.08
Average Chestnut Oak (n = 25)	0.72359 $\pm$ 0.00024	1335 $\pm$ 35	0.03 $\pm$ 0.002
Range Chestnut Oak	0.72101 to 0.72484	1080 to 1762	0.02 to 0.05
Average Red Oak (n = 26)	0.72364 $\pm$ 0.00058	1382 $\pm$ 47	0.56 $\pm$ 0.031
Range Red Oak	0.72275 to 0.72472	1036 to 1799	0.01 to 0.06

<sup>a</sup> The 'n.d.' term refers to a sample where a measurement was not determined.

$^{87}\text{Sr}/^{86}\text{Sr}$  ratios in leaves and sapwaters correlate less closely with those in exchangeable soil mineral horizons and deep soil porewaters, possibly indicating that influences of litter returns on Sr isotope composition for these reservoir components become less important with increased sampling depth. A  $\text{NH}_4\text{OAc}/\text{HOAc}$  leach procedure was applied to "carbonate free" drill core samples (DC 1–21, –29, –33, –36, Table 8) from which Sr isotope ratios were measured in order to determine a value for 'weathered' shale. Interestingly, Sr isotope ratios of soil horizons and porewaters sampled at deep depths correlate more closely with the average  $^{87}\text{Sr}/^{86}\text{Sr}$  ratio for 'weathered' shale ( $^{87}\text{Sr}/^{86}\text{Sr} = 0.72967$ ) than those observed for leaves and sap waters ( $^{87}\text{Sr}/^{86}\text{Sr} = 0.72311$ ). Another explanation for observed differences in  $^{87}\text{Sr}/^{86}\text{Sr}$  ratio as a function of depth is variability in the proportion of Sr derived from atmospheric sources. Based on results from end-member mixing calculations (Eqs. (2) and (5)), organic horizons and shallow soil porewaters at all locations are found to have less radiogenic isotope compositions and derive greater proportions of Sr from atmospheric sources. These results are not surprising given the close proximity of organic horizons and shallow soil porewaters to the surface. Proportions of atmospheric Sr ( $X(\text{Sr})_{\text{atm}}$ ) in ridge top, mid slope, and valley floor organic horizons of southern planar exchangeable soils are 0.34, 0.44, and 0.39, respectively, compared to 0.33, 0.28, and 0.25 in mineral horizons. For ridge top, mid slope, and valley floor shallow southern planar soil porewaters  $X(\text{Sr})_{\text{atm}} = 0.26, 0.39,$  and 0.35, respectively, while  $X(\text{Sr})_{\text{atm}} = 0.25, 0.31,$  and 0.31 for soil porewaters sampled

**Table 5**Average  $^{87}\text{Sr}/^{86}\text{Sr}$ , Ca/Sr, and Ge/Si ratios for sugar maple, chestnut oak, and red oak sap waters sampled at mid slope positions in various quadrants of the catchment.

Tree species	$^{87}\text{Sr}/^{86}\text{Sr}$	Ca/Sr (molar)	Ge/Si ( $\mu\text{mol}/\text{mol}$ )
<i>Northeastern</i>			
Sugar Maple (n = 4)	0.72312 $\pm$ 0.00012	421 $\pm$ 83	0.04
Chestnut Oak (n = 6)	0.72434 $\pm$ 0.00049	432 $\pm$ 68	0.04 $\pm$ 0.009
Red Oak (n = 6)	0.72366 $\pm$ 0.00060	247 $\pm$ 13	0.57 $\pm$ 0.078
<i>Northwestern</i>			
Sugar Maple (n = 6)	0.72224 $\pm$ 0.00015	417 $\pm$ 82	0.04
Chestnut Oak (n = 3)	0.72193	550 $\pm$ 106	0.05 $\pm$ 0.003
Red Oak (n = 6)	0.72062 $\pm$ 0.00014	646 $\pm$ 136	0.47 $\pm$ 0.076
<i>Southeastern</i>			
Sugar Maple (n = 4)	0.72322 $\pm$ 0.00068	293 $\pm$ 59	0.06
Chestnut Oak (n = 4)	0.72228 $\pm$ 0.00097	482 $\pm$ 115	0.06 $\pm$ 0.003
Red Oak (n = 6)	0.72312 $\pm$ 0.00107	390 $\pm$ 68	0.47 $\pm$ 0.031
<i>Southwestern</i>			
Sugar Maple (n = 3)	0.72188 $\pm$ 0.00047	426 $\pm$ 79	0.05
Chestnut Oak (n = 6)	0.72152 $\pm$ 0.00028	320 $\pm$ 26	0.05 $\pm$ 0.013
Red Oak (n = 4)	0.72075 $\pm$ 0.00018	362 $\pm$ 96	0.49 $\pm$ 0.072
<i>All locations</i>			
Average Sugar Maple (n = 17)	0.72257 $\pm$ 0.00027	393 $\pm$ 38	0.05 $\pm$ 0.011
Range Sugar Maple	0.72102 to 0.72451	189 to 702	0.01 to 0.09
Average Chestnut Oak (n = 17)	0.72246 $\pm$ 0.00043	426 $\pm$ 39	0.05 $\pm$ 0.004
Range Chestnut Oak	0.72078 to 0.72521	215 to 747	0.01 to 0.07
Average Red Oak (n = 22)	0.72205 $\pm$ 0.00045	416 $\pm$ 53	0.50 $\pm$ 0.032
Range Red Oak	0.72033 to 0.72508	219 to 1010	0.31 to 0.78

at deeper depths in corresponding locations. In shallow south swale ridge top, mid slope, and valley floor soil porewaters  $X(\text{Sr})_{\text{atm}} = 0.30$ , 0.28, and 0.35, respectively, compared to  $X(\text{Sr})_{\text{atm}} = 0.21$ , 0.21 and 0.27 for soil porewaters collected at deeper depths in corresponding locations.

In contrast, Ca/Sr and Ge/Si ratios for exchangeable soils and soil porewaters vary considerably as a function of depth for all sampling sites (Tables 1 and 2, Figs. 6 and 7). Indeed, solutes added via atmospheric sources (e.g., Ca) are observed to be in high concentrations in organic horizons and shallow porewaters, while solutes incorporated through weathering processes (e.g., Si) are enriched in mineral horizons. Further, shallow porewaters are highly influenced by biological

processes at the surface such as plant preferential discrimination of Sr and Ge relative to Ca and Si, respectively. With increased sampling depth, mineral horizons are largely separated from these processes and are primarily affected by weathering processes. In the case of porewater Ca/Sr ratio, spatial heterogeneity in total organic matter content distribution (Andrews et al., 2011) may also contribute to the observed variability with depth.

Temporal changes in porewater  $^{87}\text{Sr}/^{86}\text{Sr}$  are minor (Appendix A). In fact, fitting individual porewater  $^{87}\text{Sr}/^{86}\text{Sr}$  ratios sampled from identical sites and depths during one month of the growing season against corresponding  $^{87}\text{Sr}/^{86}\text{Sr}$  ratios measured during a separate month yields a correlation with an  $R^2$  value of 0.99. Observed decreases in porewater

**Table 6**

Seasonal silicon and calcium concentrations for sugar maple, chestnut oak, and red oak leaves sampled at mid slope positions in various quadrants of the catchment.

Tree species	June Average [Si] (mg/g dry leaf)	July Average [Si] (mg/g dry leaf)	August Average [Si] (mg/g dry leaf)	September Average [Si] (mg/g dry leaf)	June Average [Ca] (mg/g dry leaf)	July Average [Ca] (mg/g dry leaf)	August Average [Ca] (mg/g dry leaf)	September Average [Ca] (mg/g dry leaf)
<i>Northeast</i>								
Sugar Maple (n = 4)	1.45	1.87 $\pm$ 0.32	2.53	1.79	10.07	9.71 $\pm$ 0.37	n.d. <sup>α</sup>	20.88
Chestnut Oak (n = 6)	0.57	1.08	1.15 $\pm$ 0.10	1.24 $\pm$ 0.05	10.96	11.34	9.98 $\pm$ 0.13	10.75 $\pm$ 0.71
Red Oak (n = 7)	0.07	0.15 $\pm$ 0.02	0.18 $\pm$ 0.03	0.39 $\pm$ 0.03	5.69	13.75 $\pm$ 0.89	11.97 $\pm$ 1.68	12.98 $\pm$ 2.65
<i>Northwest</i>								
Sugar Maple (n = 6)	n.d. <sup>α</sup>	1.59 $\pm$ 0.03	1.85	1.59 $\pm$ 0.26	n.d. <sup>α</sup>	11.90 $\pm$ 1.53	12.17 $\pm$ 2.34	14.57 $\pm$ 3.01
Chestnut Oak (n = 4)	0.54	0.98	1.5	1.0	13.96	15.87	19.88	20.05
Red Oak (n = 6)	n.d. <sup>α</sup>	0.11 $\pm$ 0.01	0.19 $\pm$ 0.02	0.43 $\pm$ 0.12	n.d. <sup>α</sup>	10.00 $\pm$ 1.61	10.49 $\pm$ 0.51	9.15 $\pm$ 1.01
<i>Southeast</i>								
Sugar Maple (n = 6)	1.26 $\pm$ 0.22	1.60 $\pm$ 0.17	1.61 $\pm$ 0.05	n.d. <sup>α</sup>	6.40 $\pm$ 0.14	8.11 $\pm$ 2.19	8.40 $\pm$ 1.52	n.d. <sup>α</sup>
Chestnut Oak (n = 8)	0.30	0.71 $\pm$ 0.09	1.25 $\pm$ 0.11	1.36 $\pm$ 0.13	n.d. <sup>α</sup>	10.12 $\pm$ 0.91	8.01 $\pm$ 0.43	12.68 $\pm$ 1.07
Red Oak (n = 6)	n.d. <sup>α</sup>	0.13 $\pm$ 0.01	0.22 $\pm$ 0.03	0.3	n.d. <sup>α</sup>	8.15 $\pm$ 1.29	8.11 $\pm$ 0.26	11.23 $\pm$ 3.00
<i>Southwest</i>								
Sugar Maple (n = 6)	1.62 $\pm$ 0.06	1.84 $\pm$ 0.06	2.10 $\pm$ 0.25	1.74	9.96	14.79 $\pm$ 1.50	14.31 $\pm$ 0.12	19.39
Chestnut Oak (n = 7)	0.30	0.76 $\pm$ 0.05	1.10 $\pm$ 0.23	1.28 $\pm$ 0.03	9.02	10.33 $\pm$ 0.70	9.39 $\pm$ 1.43	12.02 $\pm$ 1.75
Red Oak (n = 7)	0.07	0.14 $\pm$ 0.00	0.16 $\pm$ 0.03	0.20 $\pm$ 0.05	9.04	9.96 $\pm$ 0.25	9.11 $\pm$ 1.25	11.52 $\pm$ 2.31
<i>All locations</i>								
Sugar Maple (n = 22)	1.44 $\pm$ 0.10	1.73 $\pm$ 0.08	2.03 $\pm$ 0.20	1.71 $\pm$ 0.06	8.21 $\pm$ 1.05	11.12 $\pm$ 1.11	11.62 $\pm$ 1.31	17.35 $\pm$ 2.05
Chestnut Oak (n = 25)	0.43 $\pm$ 0.07	0.88 $\pm$ 0.09	1.25 $\pm$ 0.09	1.22 $\pm$ 0.08	9.69 $\pm$ 1.92	11.35 $\pm$ 0.97	10.33 $\pm$ 0.46	13.08 $\pm$ 1.13
Red Oak (n = 26)	0.07 $\pm$ 0.00	0.13 $\pm$ 0.01	0.19 $\pm$ 0.01	0.33 $\pm$ 0.05	7.37 $\pm$ 1.68	10.46 $\pm$ 0.88	9.92 $\pm$ 0.69	11.22 $\pm$ 1.03

<sup>α</sup> The 'n.d.' term refers to months when silicon concentrations were not determined for a designated leaf sample.

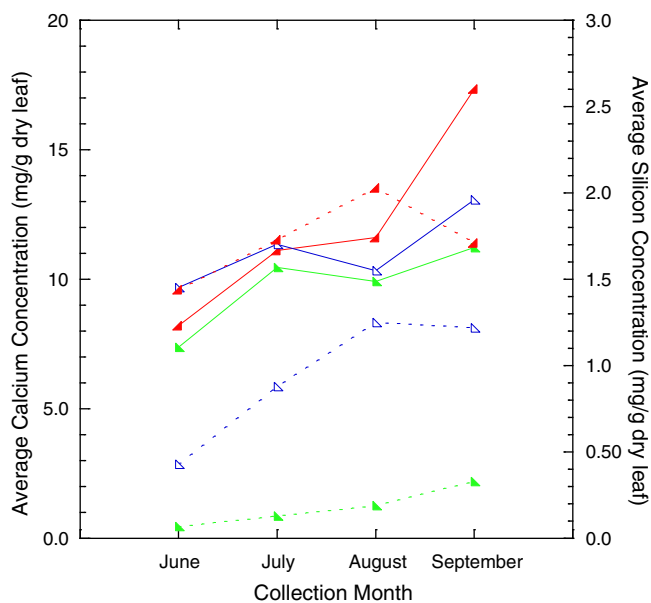


Fig. 8. Monthly average leaf [Ca] and [Si] for sugar maple (red), chestnut oak (blue), and red oak (green) species. Solid lines connect leaf [Ca], while dashed lines connect leaf [Si].

Ca/Sr ratio and increases in Ge/Si ratio (Table 3) can result from plant preferential uptake of Ca and Si over the course of the growing season. Fractionation factors (Eq. (7)) are less than one for maple ( $K_{Sr/Ca}$  range: 0.42 to 0.48 and  $K_{Ge/Si}$  range: 0.01 to 0.03) and oak ( $K_{Sr/Ca}$  range: 0.19 to 0.24 and  $K_{Ge/Si}$  range: 0.01 to 0.03 for chestnut oak and 0.18 to 0.33 for red oak) species. Higher levels of evapotranspiration over the course of the growing season enhance plant uptake of Ca and Si over Sr and Ge, depleting porewaters in Ca and Si and increasing their Sr/Ca and Ge/Si ratios. This is exaggerated in the case of Si and Ge as a strong positive relationship exists between transpiration rate and Si uptake in plants at the catchment (Meinzer et al., 2013). Observed monthly increases in porewater Ge/Si ratio may also be influenced by seasonal changes in dissolved Si source to porewaters, with phylolith dissolution contributing more significantly earlier in the season presumably due to higher levels of precipitation and larger fluxes of water passing through the soil profile where protonation of exchange sites by precipitation (pH ~4.5, NADP, 2013) will release Si as  $Si(OH)_4$  (Jin et al., 2011b; Herndon et al., 2015).

### 5.1.2. Groundwaters and streamwaters

Significantly lower  $^{87}Sr/^{86}Sr$  ratios in groundwaters and streamwaters relative to ridge top and mid slope exchangeable soils,

soil porewaters, and vegetation (Tables 1, 2, 4, 5, 7, Fig. 2) suggest that a source less radiogenic than shale is affecting Sr concentrations and Sr isotope compositions in streamwaters and groundwaters. Relatively alkaline streamwaters and groundwaters with high Ca and Mg concentrations (Table 7, Jin et al., 2011b) compared to precipitation, soils, and soil porewaters lend support to the hypothesis that lower Sr isotope compositions in groundwaters and streamwaters are resulting from the dissolution of carbonates in the catchment. As mentioned earlier, carbonates (i.e., ankerite and calcite) have been identified in the deepest samples of the DC 1 ridge top drill core (DC 1–37 and DC 1–38, Jin et al., 2010) and for all samples analyzed from the DC 3 valley floor drill core (DC 3–0–1 to DC 3–52–53, Brantley et al., 2013). In general, carbonate dissolution proceeds more rapidly than silicate mineral weathering due to the greater reactivity and solubility of carbonate minerals relative to silicate minerals. This is particularly true in a weathering limited system such as the SSHCZO where the kinetics of clay dissolution are slow (Jin et al., 2010). Thus, even a small amount of carbonate underlying streamwaters and groundwaters at the catchment has the potential of shifting  $^{87}Sr/^{86}Sr$  signatures to significantly lower values.

End-member mixing calculations indicate significant proportions of Sr derived from carbonate weathering sources in groundwaters at the catchment (range: 0.76 to 0.87 and 0.67 to 0.70 for borehole and well groundwaters, respectively). This contrasts with minor Sr contributions from silicate mineral weathering (range: 0.10 to 0.18 and 0.13 to 0.16 for borehole and well groundwaters, respectively) and atmospheric sources (range: 0.02 to 0.06 for borehole groundwaters and 0.16 for all well groundwaters). Furthermore, proportions of Sr derived from carbonate weathering sources increase from stream headwater (0.30) to mid stream (0.50) to weir locations (0.77). Concomitant decreases in Sr isotope ratio, increases in Ca/Sr ratio, increases in Ca, Sr, and Mg concentrations, and increases in pH are observed for streamwaters in the progression from stream headwater to mid stream to weir locations (Table 7 and Jin et al., 2011b). These findings complement field observations suggesting greater influxes of carbonate affected groundwaters to streamwaters at the weir location. In streamwaters, lower proportions of Sr derived from silicate weathering (0.19, 0.15, and 0.07 for stream headwater, mid stream, and weir locations, respectively) relative to atmospheric (0.50, 0.35, and 0.16 for stream headwater, mid stream, and weir locations, respectively) sources are consistent with the slow kinetics of clay dissolution at the catchment (Jin et al., 2010). High proportions of atmospherically derived Sr in stream headwaters agree with field observations which indicate stream flow at this location to occur exclusively during snowmelt and rainstorms in the early spring and fall (Jin et al., 2011b). Mid stream locations presumably integrate biogeochemical processes at upstream (i.e., stream headwater) and downstream (i.e., weir) locations (Table 7) where proportions of Sr derived from carbonate weathering, silicate weathering, and atmospheric sources in streamwaters at the mid stream location are in between the proportions determined for streamwaters sampled at stream headwater and weir locations. However, Ca/Sr ratios and Ca, Sr and Mg

Table 7  
Strontium, calcium, chloride, silicon, and germanium concentrations, pH values, and Ca/Sr,  $^{87}Sr/^{86}Sr$ , ( $^{87}Sr/^{86}Sr$ )\*, and Ge/Si ratios for groundwaters and streamwaters sampled at the catchment on October 8, 2013.

Sample ID	Depth to water from top of casing (cm)	pH	Sr ( $\mu M$ )	Ca ( $\mu M$ )	Ca/Sr (molar)	Cl <sup>a</sup> ( $\mu M$ )	$^{87}Sr/^{86}Sr$	( $^{87}Sr/^{86}Sr$ )*	Si ( $\mu M/kg$ )	Ge (pM/kg)	Ge/Si ( $\mu mol/mol$ )
CZMW 1	91	8.08	3.08	1070	347	23.7	0.71481	0.71492	112	n.d. <sup>b</sup>	n.d. <sup>b</sup>
CZMW 6	849	6.25	1.37	948	692	24.4	0.71746	0.71787	169	n.d. <sup>b</sup>	n.d. <sup>b</sup>
Well 8	230	6.62	0.34	195	568	17.7	0.71683	0.71805	127	n.d. <sup>b</sup>	n.d. <sup>b</sup>
Well 11	478	6.44	0.11	81	708	n.d. <sup>b</sup>	0.71585	0.71688	114	86	0.75
Well 13	276	6.68	0.46	631	1383	23.8	0.71577	0.71678	118	79	0.70
Weir Streamwater	0	6.07	0.83	871	1044	43.2	0.71362	0.71422	128	93	0.73
Mid Stream	0	n.d. <sup>b</sup>	0.37	227	601	41.7	0.71610	0.71914	127	111	0.90
Stream Headwater	0	5.80	0.25	155	610	40.2	0.71758	0.72475	126	249	1.98

\*The chloride normalized  $^{87}Sr/^{86}Sr$  ratio for a designated sample.

<sup>a</sup> Chloride elemental concentrations provided by P. Sullivan, (unpublished data).

<sup>b</sup> The 'n.d.' term refers to a sample where a measurement was not determined.

**Table 8**

$^{87}\text{Sr}/^{86}\text{Sr}$ , Ca/Sr, and Ge/Si ratios for drill cores sampled at the ridge top borehole (DC 1) and at the CMZW 2 borehole near the stream's weir (DC 3) on May 21, 2014. Quantitative mineralogy for DC 1 and DC 3 samples from Jin et al. (2010), and Brantley et al. (2013) are shown for reference.

Sample ID	Depth (cm)	$^{87}\text{Sr}/^{86}\text{Sr}$ (carbonate fraction)	Ca/Sr (molar) (carbonate fraction)	$^{87}\text{Sr}/^{86}\text{Sr}$ (silicate fraction)	Ca/Sr (molar) (silicate fraction)	Ge/Si ( $\mu\text{mol}/\text{mol}$ ) (silicate fraction)	Calcite and Ankerite (wt.%) <sup>a</sup>
DC 1–21	465	0.72922	409	0.74537	13	n.d. <sup>b</sup>	0
DC 1–29	1074	0.72833	545	0.74497	11	n.d. <sup>b</sup>	0
DC 1–33	1684	0.73087	376	0.74806	34	n.d. <sup>b</sup>	0
DC 1–36	2143	0.73026	951	0.74919	34	n.d. <sup>b</sup>	0
DC 1–37	2294	0.71935	2865	0.74720	89	n.d. <sup>b</sup>	1.6 <sup>6</sup>
DC 1–38	2446	0.71910	2899	0.74143	398	n.d. <sup>b</sup>	7.8 <sup>6</sup>
DC 3–4–5	137	0.71181	849	0.74310	38	2.09	0.6
DC 3–5–6	168	0.71222	734	0.74297	22	1.99	4.0
DC 3–8–9	259	0.71180	760	0.74415	31	1.99	2.6
DC 3–21–22	655	0.70812	789	0.74501	79	2.12	17.3
DC 3–22–23	686	0.70987	1110	0.74718	33	2.04	3.6
DC 3–42–43	1296	0.71408	1049	0.74834	112	1.77	3.1

<sup>a</sup>Ankerite carbonate composition as inferred from high Fe, Mn, and Ca elemental compositions, high LOI content, and the grey coloration of samples (Jin et al., 2010).

<sup>a</sup> Quantitative mineralogy for DC 1 and DC 3 samples derived from Jin et al. (2010) and Brantley et al. (2013).

<sup>b</sup> The 'n.d.' term refers to a sample where a measurement was not determined.

concentrations in mid streamwaters are remarkably similar to those observed in streamwaters at the upslope headwater location due to the direction of fluid motion and are significantly lower than values reported for weir streamwaters where carbonate affected groundwater recharge strongly influences solute chemistry.

For streamwaters at weir, mid stream, and stream headwater locations, total Sr fluxes are estimated to be 3.22, 0.97, and 0.79 mol ha<sup>-1</sup> yr<sup>-1</sup>, respectively. Atmospheric Sr flux estimates for weir, mid stream, and head streamwaters are 0.53, 0.35, and 0.40 mol ha<sup>-1</sup> yr<sup>-1</sup>, respectively. Sr flux estimates to weir, mid stream, and head streamwaters from carbonate weathering sources are 2.68, 0.49, and 0.24 mol ha<sup>-1</sup> yr<sup>-1</sup>, while those from silicate weathering sources are 0.01, 0.14, and 0.15 mol ha<sup>-1</sup> yr<sup>-1</sup>, respectively. Total Ca fluxes of 2499, 635, and 436 mol ha<sup>-1</sup> yr<sup>-1</sup> are estimated for streamwaters at weir, mid stream, and stream headwater locations, respectively. Ca fluxes from atmospheric sources in streamwaters at weir, mid stream, and stream headwater locations are estimated to be 122, 80, and 92 mol ha<sup>-1</sup> yr<sup>-1</sup>, respectively. Ca flux estimates to weir, mid stream, and head streamwaters from carbonate weathering sources are 2365, 546, and 332 mol ha<sup>-1</sup> yr<sup>-1</sup>, respectively, while those derived from silicate weathering sources are 12, 9, and 12 mol ha<sup>-1</sup> yr<sup>-1</sup>. Although not directly apparent from Ca/Sr ratios, both Ca and Sr concentrations (Table 7) and fluxes in streamwaters are observed to increase from stream headwater to mid stream to weir locations. Jin et al. (2011b) observed a similar pattern for Mg in streamwaters at Shale Hills where increases downstream are similarly attributed to more substantial contributions by carbonate-affected groundwaters to weir streamwaters.

Ge/Si ratios for groundwaters and weir and mid streamwaters are lower than those determined for unweathered shale (Tables 7 and 8, Fig. 4). Incidentally, the average groundwater Ge/Si ratio is found to be identical to the value determined for weir streamwaters. This is consistent with Sr isotope and Ca/Sr ratios and elemental concentrations that suggest groundwater to be an important source of solutes to the weir location. In contrast, stream headwaters display a Ge/Si ratio similar to the average value for unweathered bedrock. However, this ratio also corresponds reasonably well to values determined for shallow southern quadrant valley floor porewaters. As mentioned previously, the stream headwater position is transient and flows only during snowmelt and rainstorms (Jin et al., 2011b). Dissolved Si and Ge concentrations in precipitation are insignificant (Bartoli, 1983; Mortlock and Froelich, 1987; Garvin, 2006). Thus, one hypothesis would be that the high Ge/Si ratio for stream headwaters is a result of flushing of Ge enriched soil porewaters (Table 1) by infiltrating precipitation. Cl normalized  $^{87}\text{Sr}/^{86}\text{Sr}$  ratios were determined to correct for atmospheric contributions of Sr in stream headwaters and resemble those of nearby north swale valley floor leaves (Tables 4 and 7). As leaves at the

catchment largely derive solutes from shallow soil exchangeable pool and porewater sources, the similarity in  $^{87}\text{Sr}/^{86}\text{Sr}$  ratio between stream headwaters and leaves also suggest a possible soil porewater source of Sr to stream headwaters. This agrees with studies at Shale Hills which have suggested that organic-rich swales and surface soils are an important source of solutes to the stream during dry and wet periods while organic-poor hillslope soils contribute solutes during rain events (Qu and Duffy, 2007; Andrews et al., 2011; Herndon et al., 2015).

#### 5.2. Ca-Sr and Ge-Si fractionation between soil and biomass reservoirs

Average leaf Ca/Sr and Ge/Si ratios are significantly higher and lower, respectively, than those determined for exchangeable soils, soil porewaters, sap waters, streamwaters, groundwaters, and bedrock (Tables 1, 2, 4, 5, 7, and 8, Figs. 3 and 4). Partitioning between Ca-Sr and Ge-Si is observed in numerous plant species sampled across a wide range of ecosystems (Poszwa et al., 2000; Watmough and Dillon, 2003; Blecker, 2005; Bullen and Bailey, 2005; Derry et al., 2005; Garvin, 2006; Drouet and Herbauts, 2008; Delvigne et al., 2009; Sparks et al., 2010; Pett-Ridge et al., 2009). For Ca and Sr, sugar maple leaves in southwestern and southeastern quadrants have higher fractionation factors (0.48 and 0.43, respectively) and discriminate to a lesser degree against Sr than chestnut oak (0.24 and 0.19, respectively) and red oak (0.22 and 0.19, respectively) leaves. Greater preferential discrimination against Sr in oak relative to maple leaves is likely related to physiological differences between the two species and is consistent with findings from other studies conducted in the northeastern United States (Blum et al., 2008, 2012; Lucash et al., 2012). Given Sr's utility as a tracer for Ca in catchment studies (Miller et al., 1993; Bailey et al., 1996; Kennedy et al., 2002; Bullen and Bailey, 2005; Blum et al., 2008; Pett-Ridge et al., 2009), similarities in Sr isotope ratio among foliage derived from maple and oak species (Table 4, Fig. 2) seem to imply that discrepancy in foliar Ca/Sr ratio among species is reflective of variable degrees of uptake rather than different sources from which plants are acquiring solutes. Variation in partitioning between Ca and Sr among tree species growing in the same soil agrees with findings from other studies (Runia, 1987; Veresoglou et al., 1996; West et al., 2001; Drouet and Herbauts, 2008; Blum et al., 2012). For Ge and Si, red oak leaves in southwestern and southeastern quadrants have higher average fractionation factors (0.28 and 0.25, respectively) and discriminate to a lesser degree against Ge than sugar maple (0.01 and 0.01, respectively) and chestnut oak (0.01 and 0.01, respectively) leaves. As discussed by Sparks et al. (2010), such significant differential uptake of Si relative to Ge, as is observed in maple and chestnut oak species, is best explained by active, plant-mediated transport mechanisms which are highly specific (Clarkson, 1993; White, 2001) rather than by molecular diffusion processes or energetic differences between amorphous SiO<sub>2</sub> and GeO<sub>2</sub>.

Interestingly, average Ca/Sr ratios in sap waters are significantly lower than those observed in paired leaf samples (Tables 1, 4 and 5, Fig. 3). Instead, sap water Ca/Sr ratios are comparable to porewater Ca/Sr ratios sampled at similar locations. For example, average Ca/Sr ratios for sugar maple, chestnut oak, and red oak sap waters collected at mid slope locations of the southwestern quadrant correspond reasonably well to the average Ca/Sr ratio for mid slope porewaters (Tables 1 and 5). Average Ca/Sr ratios for sugar maple, chestnut oak, and red oak sap waters collected at mid slope locations of the southeastern quadrant are generally similar to the average Ca/Sr value for southwale mid slope shallow porewaters (Tables 1 and 5). Tree transpiration processes were shown to concentrate Ca and Sr in sap waters to similar degrees. For example, average southwestern sap water Sr and Ca concentrations in maple species (1.46 and 521  $\mu\text{M}$ , respectively) were observed to be 13–14 times larger, while those in oak species ( $2.30 \pm 0.06$  and  $793 \pm 12 \mu\text{M}$ , respectively) were observed to be 20–21 times larger, than those in corresponding southern planar mid slope soil porewaters (0.11 and 38  $\mu\text{M}$ ). Observations of similar Ca/Sr ratios in sap waters compared to source porewaters and accumulation of Ca and Sr by plant species growing in the same substrate suggest limited competition between these divalent cations during transport (Wyttenbach et al., 1995; Veresoglou et al., 1996; Dasch et al., 2006; Drouet and Herbauts, 2008). Considering that the apoplastic pathway is relatively non-selective between divalent cations (White, 2001; White et al., 2002; White and Broadley, 2003), transport of Ca through the root to the xylem is hypothesized to occur largely along apoplastic rather than the highly selective symplastic pathways as has been suggested by other researchers (Clarkson, 1984; McLaughlin and Wimmer, 1999; White, 2001; White et al., 2002). Nonetheless, fractionation between Ca and Sr must take place further along the transpiration stream as evidenced by the higher Ca/Sr ratios observed in leaf tissues relative to source porewaters (Tables 1 and 4). As indicated earlier, the xylem transports Ca (and by inference, Sr) ions towards rapidly transpiring organs such as leaves. During transport, increased translocation of Ca relative to Sr, with Sr retained by cation exchange sites to a greater degree than Ca on cell walls of xylem vessels and surrounding tissues, has been suggested to occur during apoplastic transport through the xylem to above ground leaf components (Clarkson, 1984; Wolterbeek et al., 1984; Veresoglou et al., 1996; Bailey et al., 1996; Dasch et al., 2006; Drouet and Herbauts, 2008). Previous studies have argued that discrimination between Ca and Sr is the result of preferential Ca binding in calcium oxalate complexes which are released by bark or other plant tissues and accumulate in leaf mesophyll cells (McNair, 1932; Gulpin et al., 1995; Funk and Amatangelo, 2013).

In contrast, average Ge/Si ratios for sap waters correspond more closely to leaves than soil porewaters (Tables 1, 4, and 5, Fig. 4). These findings agree with those presented by Garvin (2006); Blecker et al. (2007), and Delvigne et al. (2009) where Ge/Si ratios for stem xylem water derived from sugar maple trees, grasses, bananas, and horsetails were remarkably similar to those reported for leaves. Such minimal discrepancy between leaf and sap water Ge/Si ratios, where Ge/Si ratios for both are significantly lower than those for soil porewaters, suggest that Ge/Si fractionation must precede phytolith formation and occur en route from the endodermal cell layer (and casparian strip) to the xylem stream, as proposed by Sparks et al. (2010).

Over the growing season, Ca and Si accumulate in leaf tissue for all tree species (Table 6, Fig. 8) consistent with findings by other studies for higher plants conducted in similar canopy settings (Schlesinger, 1997; Garvin, 2006). However, it should be noted that decreases in leaf Si concentration for sugar maple and chestnut oak species from August to September (Fig. 8) are likely due to recycling of biogenic Si to soil reservoirs during early leaf fall. Garvin (2006) and Carnelli et al. (2001) have attributed monthly Si increases to constant inputs from waters transporting Si to leaves by means of the transpiration pathway. This is reasonable considering Si's nature as an uncharged molecule (silicic acid,  $\text{H}_4\text{SiO}_4$ ) where its translocation in plant tissue is more

dependent on the transpiration stream than other chemical species. Complementing this are enhanced levels of evapotranspiration over the course of the growing season, as inferred from shallow soil water  $\delta^{18}\text{O}$  and  $\delta^2\text{H}$  values, which facilitate transpiration processes, and hence, the preferential uptake of Ca over Sr and Si over Ge from porewater reservoirs by plants at the catchment. Additionally, Ca and Si concentrations generally increase with leaf age because these elements cannot be remobilized for retranslocation to other plant tissues once deposited in leaves (Jarvis, 1987; McLaughlin and Wimmer, 1999; Ma and Yamaji, 2006). The maturation of leaves is also responsible for inhibiting the formation of a sink from which apoplastic binding locations can release Ca and Si bound in the xylem walls to result in higher Ca and Si levels present in xylem sap water in the late summer/early fall (de Bakker et al., 1999; Ma and Yamaji, 2006). In studies at Shale Hills, Meinzer et al. (2013) demonstrated that transpiration rates in diffuse-porous maple species were responsive to fluctuations in soil moisture (i.e., isohydric), while ring porous oak species were relatively unaffected by soil moisture content (i.e., anisohydric) which is consistent with findings by other researchers (Abrams, 1990; Tardieu and Simonneau, 1998; Ewers et al., 2007). As Ca and Si fluxes to the xylem are highly influenced by transpiration, monthly changes in Ca/Sr and Ge/Si ratio are reasonable for species whose transpiration rates vary over the course of the growing season.

### 5.3. Mineralogical influences on drill core chemistry

The average  $^{87}\text{Sr}/^{86}\text{Sr}$  ratio for the carbonate fraction of DC 1 carbonate bearing ridge top drill core samples (DC 1–37 and DC 1–38) is significantly higher than the value determined for drill core samples collected from the DC 3 valley floor location (Table 8, Fig. 2). This observation reflects differences in the composition of carbonates between sites possibly due to the heterogeneous lithology of the Rose Hill formation (Flueckinger, 1969). Similar  $^{87}\text{Sr}/^{86}\text{Sr}$  ratios observed in carbonate affected DC 1 drill core samples (Table 8) imply that a single carbonate source is affecting Sr isotope compositions at this location. The variation in Sr isotope ratio for the carbonate fraction of DC 3 valley floor drill core samples (Table 8) suggest multiple carbonate sources of Sr. Previous work has shown that carbonates obtained from the DC 1 drill core are ankerite ( $\text{Ca}(\text{Mg}, \text{Fe}, \text{Mn})(\text{CO}_3)_2$ ), while those collected from the DC 3 drill core are a mixture of calcite and ankerite (Jin et al., 2010; Brantley et al., 2013). According to major element data obtained from carbonate fractions of DC 1 and DC 3 drill cores (Appendix A), reasonably high Fe and Mg concentrations were reported for samples collected from the deepest depths (i.e. DC 1–38 and DC 3–42–43). Specifically, Fe concentrations of 31.30 and 21.15 mmol/kg were reported for DC 1–38 and DC 3–42–43, respectively, while corresponding Mg concentrations were found to be 32.47 and 15.45 mmol/kg, respectively. At the DC 3 site, average carbonate  $\delta^{13}\text{C}$  compositions ( $-1.1 \text{‰}$ ) better resemble values for marine carbonates ( $\sim 0$ ) than those for DC 1 carbonates ( $-5.9 \text{‰}$ ) (Jin et al., 2014). Furthermore, Brantley et al. (2013) observed precipitation of secondary calcites at depths below the valley floor carbonate weathering front ( $\sim 4$  m depth) with dissolution of carbonates above this depth likely due to their fast dissolving nature in the local equilibrium regime of the catchment. As such, ankerites are hypothesized to be largely contributing to the  $^{87}\text{Sr}/^{86}\text{Sr}$  ratio at the DC 1 ridge top site with influences on Sr isotope signature by secondary calcites assumed to be significant at the DC 3 valley floor site. Hence, at least two mineralogically and isotopically distinct generations of diagenetic or secondary carbonates are present at the catchment.

For the carbonate fraction of drill core samples at the DC 3 site, greater variability in Sr isotope composition as a function of depth (Table 8) is attributed to differences in relative proportions of Sr derived from calcite and ankerite. Increased proportions of calcite and ankerite, as determined in quantitative XRD patterns (Jin et al., 2010; Brantley et al., 2013), generally correlate with lower Sr isotope ratios for DC 3 valley floor drill core samples (Table 8). A narrow range of Sr isotope

ratios is found for “carbonate free” DC 1 samples; hence, the minimal variation observed in  $^{87}\text{Sr}/^{86}\text{Sr}$  ratio from 465 cm to the 2143 cm depth (Table 8). At the 2294 cm depth, the presence of ankerite significantly lowers the  $^{87}\text{Sr}/^{86}\text{Sr}$  ratio for the DC 1–37 drill core sample (Table 8). Minimal variation is observed in  $^{87}\text{Sr}/^{86}\text{Sr}$  ratio between DC 1–37 and DC 1–38 drill core samples collected at the 2294 and 2446 cm depths, respectively, despite differences in ankerite content (Table 8). With the exception of DC 3–5–6 (168 cm) and DC 3–42–43 (1296 cm), spatial variation in  $^{87}\text{Sr}/^{86}\text{Sr}$  ratio can also be attributed to differences in relative proportions of carbonate present in DC 3 drill core samples. As mentioned earlier, less radiogenic calcites are hypothesized to be contributing greater proportions of Sr to DC 3 valley floor drill core samples than ankerite. Thus, concurrent decreases in Sr isotope ratio with increases in carbonate content are observed in most DC 3 samples (Table 8).

Lower  $^{87}\text{Sr}/^{86}\text{Sr}$  ratios in ‘weathered’ versus unweathered DC 1 drill core samples (Table 8) lend support to the hypothesis of Ca and Sr loss in shale through feldspar (i.e., plagioclase) dissolution. Progression of feldspar dissolution before clay mineral weathering is based on mineralogical observations at the catchment (Jin et al., 2010) which indicate that soil cores are depleted in Na and Ca but not in K, Mg, Al, and Fe relative to unweathered material from drill cores. Additionally, significantly positive Eu anomalies in natural waters and exchangeable pools at Shale Hills (Ma et al., 2011a; Ma et al., 2011b) suggest preferential dissolution of plagioclase feldspar during chemical weathering. The lower  $^{87}\text{Sr}/^{86}\text{Sr}$  ratio of the “carbonate free” DC 1 samples relative to shales is inferred to result from leaching of less radiogenic Sr from feldspar dissolution or from interlayer and adsorption sites of clay minerals (i.e., illites and chlorites) which dominate the mineralogy of shales at the catchment (Jin et al., 2010). The less radiogenic isotope signature of Sr released during feldspar alteration can be incorporated into “carbonate free” DC 1 samples through exchange reactions at interlayer and adsorption sites on more radiogenic clay minerals.

For the DC 1 ridge top drill core, Ca/Sr ratios in carbonate fractions of carbonate bearing samples are predictably higher than those observed in “carbonate free” samples (Table 8, Fig. 3). Ca concentrations correspond reasonably well to proportions of carbonates estimated in DC 1 and DC 3 drill core samples through quantitative XRD patterns. Ca/Sr ratios for DC 1 ridge top drill core samples generally increase with depth, while no discernible dependence on depth is observed for drill core samples collected from the DC 3 valley floor site. Differences in Ca/Sr ratio for DC 1 and DC 3 drill core samples with depth may be due to variations in carbonate composition or degrees of  $\text{CO}_2$  acquisition and  $\text{CO}_2$  degassing as these processes lead to the dissolution and precipitation of carbonates at the catchment, respectively.

Sr isotope ratios for silicate fractions of drill core samples are rather similar between DC 1 and DC 3 sites (Table 8, Figs. 2, 3) and fall within the range of values reported for shales in the area (Whitney and Hurley, 1964). Low Ca/Sr ratios are reported for both the DC 1 and DC 3 silicate fractions of drill core samples uncontaminated by carbonates and are consistent with values calculated using major and trace element data derived from other studies at the catchment (Jin et al., 2010; Ma et al., 2011a,b). Heterogeneity in the composition of the Rose Hill shale (Lynch, 1976) may be responsible for observed spatial variability in  $^{87}\text{Sr}/^{86}\text{Sr}$  and Ca/Sr ratios for drill core samples collected from both locations. Increased porosity in the weathered zone enables precipitation to infiltrate into shale fractures or joints to accelerate mineral dissolution and fracturing and eventually leads to the disaggregation of the shale. Neutron scattering studies at the catchment (Jin et al., 2011a) suggest that in low-porosity and low-permeability bedrock between fractures fluid transport is controlled by slow diffusion processes. In this way, residence times for solutes in bedrock between fractures are long and small changes in porosity will significantly impact weathering processes. Indeed, Sr isotope ratios of ‘weathered’ shale (carbonate fraction of DC 1–21, 29, 33, 36) are less radiogenic than unweathered shale (silicate fractions of DC 1 and DC 3), while Ca/Sr ratios are higher in ‘weathered’ shale relative to unweathered shale (Table 8).

Ge/Si ratios for DC 3 drill core samples collected near the stream's weir (Table 8, Fig. 4) are consistent with those reported for shale (Mortlock and Froelich, 1987). Ge/Si ratios are rather uniform despite differences in sampling depth; however, the Ge/Si ratio of the drill core sample collected from the deepest depth (DC 3 42–43 at 1296 cm) is somewhat lower than values reported for other samples. Interestingly, Si concentrations in deep groundwaters (CZMW 6 at 849 cm) are also reported to be higher than those for shallower groundwaters (Table 7). This complements mineralogical studies at the catchment (Jin et al., 2010, 2011a; Brantley et al., 2013) which predict the onset of feldspar weathering at the valley floor to occur at a depth of ca. 700 cm. The preliminary data support the hypothesis that both Ge and Si are incorporated into natural waters from feldspar dissolution and clay neof ormation processes in DC 3 drill core samples at depths below 700 cm.

#### 5.4. Carbonate weathering front propagation rate

The rate of propagation of the carbonate weathering front for the carbonate source at the CZMW 2 borehole near the stream's weir (DC 3) is calculated using the Ca flux for calcite at the stream's weir ( $9.5 \times 10^{-4} \text{ g Ca cm}^{-2} \text{ yr}^{-1}$ ), the average density of calcite ( $1.1 \text{ g Ca cm}^{-3}$ ), and the average proportion of carbonates in DC 3 valley floor drill core samples as estimated by quantitative XRD patterns at Shale Hills (0.03125; Brantley et al., 2013). A preliminary estimate of the rate of carbonate propagation is  $\approx 280 \text{ m Myr}^{-1}$  which is 6 and 16 times larger than rates reported for regolith production at ridge top/mid slope ( $44 \text{ m Myr}^{-1}$ , Ma et al., 2010) and valley floor ( $17 \text{ m Myr}^{-1}$ , Ma et al., 2010) positions of the southern planar quadrant as calculated by U-series isotopes. Furthermore, the rate of carbonate propagation exceeds the catchment-wide erosion rate as inferred from cosmogenic  $^{10}\text{Be}$  dating of sediments ( $15 \text{ m/Myr}$ , Jin et al., 2010) by a factor of approximately 20.

Discrepancies between rates of regolith production and carbonate front propagation are consistent with greater depths inferred for carbonate weathering at the catchment (Jin et al., 2010; Jin et al., 2011a; Brantley et al., 2013). Elevated levels of Ca (Table 7) and Mg (Jin et al., 2011b) are also present in groundwaters relative to soil porewaters at Shale Hills consistent with a local equilibrium regime where erosion rates are slower than dissolution rates for carbonate minerals (Jin et al., 2010, 2011b; Brantley et al., 2013). Due to the high reactivity and solubility of carbonate minerals relative to silicate minerals, carbonates are expected to dissolve under local equilibrium (Lebedeva et al., 2010). Hence, the ‘completely developed depletion profile’ for Ca referenced in Brantley et al. (2013), where carbonates are hypothesized to be completely dissolved in the upper portion of the profile at the DC 1 ridge top (above 2200 cm) and DC 3 valley floor (above 200 cm) drill core sites. On the contrary, incompletely developed depletion profiles, where erosion rates exceed dissolution rates, are expected for silicate minerals at the catchment with these slow dissolving and abundant minerals present at the land surface (Jin et al., 2010, 2011b; Brantley et al., 2013). However, it should be noted that the timescales for regolith production and carbonate weathering front propagation vary considerably. While soil chemistry documents extents of reactions over timescales of tens of thousands of years, carbonate abundance is in part a function of groundwater flow and chemistry. Groundwater residence times are estimated to be on the order of one year as a result of the relatively shallow flowpaths for groundwaters in the fractured bedrock of the catchment (Jin et al., 2011b).

## 6. Conclusions

This study employs the use of multiple tracers ( $^{87}\text{Sr}/^{86}\text{Sr}$ , Ca/Sr, Ge/Si ratios) to examine sources and cycling of solutes at the Susquehanna/Shale Hills Critical Zone Observatory (SSHCZO). To better understand biogeochemical processes affecting the distribution and availability of

solutes in individual reservoir components, a comprehensive data set is compiled for plant leaves and sap waters and for streamwaters, groundwaters, soil porewaters, exchangeable soils, and bedrock. Understanding Ca, Sr, Ge, and Si sources and cycling in reservoir components of the SSHCZO provides a framework for future terrestrial biogeochemical models. In particular, preliminary geochemical data can be incorporated into models to visualize elemental feedback processes at the SSHCZO. By so doing, data can be extrapolated across longer time scales and broader spatial extents allowing a discussion of larger scientific issues such as the susceptibility of the ecosystem to acid deposition (Miller et al., 1993; Bailey et al., 1996; Capo et al., 1998; Likens et al., 1998; Pett-Ridge et al., 2009) or the role of silicate weathering in mediating atmospheric CO<sub>2</sub> levels for the region (Alexandre et al., 1997; Carnelli et al., 2001; Sommer et al., 2006; Street-Perrott and Barker, 2008; Cornelis et al., 2010).

<sup>87</sup>Sr/<sup>86</sup>Sr ratios for soil reservoirs at the valley floor are significantly lower than those reported at upslope locations, consistent with carbonate affected groundwater recharge to valley floor soils and soil porewaters. Biological uptake discriminates against Sr relative to Ca and Ge relative to Si, resulting in higher Ge/Si ratios and lower Ca/Sr ratios in soils compared to plant tissues. Minimal variation in leaf and sap water <sup>87</sup>Sr/<sup>86</sup>Sr ratios observed between species sampled from comparable quadrants and transect positions imply a similar source from which plants are acquiring Sr (and by inference, Ca). <sup>87</sup>Sr/<sup>86</sup>Sr ratios in plant tissues are most similar to shallow pore waters (0–50 cm), implying mineral nutrients are obtained from the near sub-surface. These findings agree with δ<sup>18</sup>O studies suggesting water uptake from a single shallow soil reservoir source by plants at the catchment.

Minimal discrepancy between leaf and sap water Ge/Si ratios, where Ge/Si ratios for both are significantly lower than those for soil porewaters, suggests that partitioning between Ge and Si precedes phytolith formation and occurs in the transport from the endodermal cell layer (and casparian strip) to the xylem stream either during plant uptake or soon thereafter. Conversely, Ca/Sr ratios in sap waters are shown to correspond more closely to those in soil porewaters with elemental partitioning occurring further along the transpiration stream. This is supported by observations of significantly higher Ca/Sr ratios in leaves compared to soil porewaters.

In groundwaters and weir streamwaters, carbonate dissolution processes are rather important sources of Ca and Sr, while the primary weathering of silicate minerals influences Si and Ge chemistry. However, stream headwaters are ephemeral and highly responsive to inputs from atmospheric sources for Ca and Sr and to hydrological processes which add Si and Ge to streamwaters through flushing by infiltrating precipitation of soil porewaters into streamwaters. Mid streamwaters integrate sources of solutes at weir and stream headwater locations.

Diagenetic carbonates include both ankerites and calcites but these have distinct <sup>87</sup>Sr/<sup>86</sup>Sr ratios and represent different alteration events. The rate of carbonate propagation exceeds those estimated for regolith production and erosion and is consistent with the greater depth inferred for the carbonate weathering front at the catchment. Sr isotope ratios for silicate fractions of drill core samples suggest that Ca and Sr release through weathering is likely from leaching of less radiogenic feldspars and from interlayer and adsorption sites of clay minerals. Ge/Si ratios from beneath the active soil zone are low relative to unweathered bedrock, indicating neof ormation of a high Ge/Si phase (probably clay) during shale weathering.

## Acknowledgments

We thank J. Pollak for his help with sampling and G. McElwee and A. Cross for their help with sample analysis. Financial support was partially provided from NSF EAR-1227107 to L.D. and J.S.

## Appendix A. Supplementary data

Supplementary data to this article can be found online at <http://dx.doi.org/10.1016/j.chemgeo.2016.04.026>.

## References

- Aberg, G., Jacks, G., Hamilton, P., 1989. Weathering rates and 87Sr/86Sr ratios: an isotopic approach. *J. Hydrol.* 109, 65–78.
- Aberg, G., 1995. The use of natural strontium isotopes as tracers in environmental studies. *Water Air Soil Pollut.* 79, 209–322.
- Abrams, M., 1990. Adaptations and responses to drought in *Quercus* species of North America. *Tree Physiol.* 7, 227–238.
- Alexandre, A., Meunier, J., Colin, F., Koud, J., 1997. Plant impact on the biogeochemical cycle of silicon and related weathering processes. *Geochim. Cosmochim. Acta* 61, 677–682.
- Andrews, D., Lin, H., Zhu, Q., Jin, L., Brantley, S., 2011. Hot spots and hot moments of dissolved organic carbon export and soil organic carbon storage in the Shale Hills catchment. *Vadose Zone J.* 10, 943–954.
- Bailey, S., Hornbeck, J., Driscoll, C., Gaudette, H., 1996. Calcium inputs and transport in a base-poor forest system as interpreted by Sr isotopes. *Water Resour. Res.* 32, 707–719.
- Bain, D., Bacon, J., 1994. Strontium isotopes as indicators of mineral weathering in catchments. *Catena* 22, 201–214.
- Bartoli, F., 1983. The biogeochemical cycle of silica in two temperate forest ecosystems. *Environ. Biogeochemistry Ecol. Bull.* 35, 469–476.
- Belanger, N., Holmden, C., Courchesne, F., Cote, B., Hendershot, W., 2012. Constraining soil mineral weathering <sup>87</sup>Sr/<sup>86</sup>Sr for calcium apportionment studies of a deciduous forest growing on soils developed from granitoid igneous rocks. *Geoderma* 185–186, 84–96.
- Bernstein, L., 1985. Germanium geochemistry and mineralogy. *Geochim. Cosmochim. Acta* 49, 2409–2422.
- Blecker, S., 2005. *Silica Biogeochemistry Across a Grassland Climosequence*. Colorado State University, Fort Collins (Ph.D. diss).
- Blecker, S., King, S., Derry, L., Chadwick, O., Ippolito, J., Kelly, E., 2007. The ratio of germanium to silicon in plant phytoliths: quantification of biological discrimination under controlled experimental conditions. *Biogeochemistry* 86, 189–199.
- Blum, J., Klaue, A., Nezat, C., Driscoll, C., Johnson, C., Siccama, T., Eagar, C., Fahey, T., Likens, G., 2002. Mycorrhizal weathering of apatite as an important calcium source in base-poor forest ecosystems. *Nature* 417, 729–731.
- Blum, J., Dasch, A., Hamburg, S., Yanai, R., Arthur, M., 2008. Use of foliar Ca/Sr discrimination and <sup>87</sup>Sr/<sup>86</sup>Sr ratios to determine soil Ca sources to sugar maple foliage in a northern hardwood forest. *Biogeochemistry* 87, 287–296.
- Blum, J., Hamburg, S., Yanai, R., Arthur, M., 2012. Determination of foliar Ca/Sr discrimination factors for six tree species and implications for Ca sources in northern hardwood forests. *Plant Soil* 356, 303–314.
- Brantley, S., Duffy, C., 2008, 2009, 2010. CZO Dataset: Shale Hills—Stream Water Chemistry. <http://criticalzone.org/shale-hills/data/dataset/2582>.
- Brantley, S., Holleran, M., Jin, L., Bazilevska, E., 2013. Probing deep weathering in the Shale Hills Critical Zone Observatory, Pennsylvania (USA). The hypothesis of nested chemical fronts in the subsurface. *Earth Surf. Process. Landf.* 38, 1280–1298.
- Bullen, T., Bailey, S., 2005. Identifying calcium sources at an acid deposition-impacted spruce forest: a strontium isotope, alkaline earth element multi-tracer approach. *Biogeochemistry* 75, 63–99.
- Capo, R., Stewart, B., Chadwick, O., 1998. Strontium isotopes as tracers of ecosystem processes: theory and methods. *Geoderma* 82, 197–225.
- Carnelli, A., Madella, M., Theurillat, J., 2001. Biogenic silica production in selected alpine plant species and plant communities. *Ann. Bot.* 87, 425–434.
- Casey, W., Kinrade, S., Knight, C., Rains, D., Epstein, E., 2003. Aqueous silicate complexes in wheat, *Triticum aestivum* L. *Plant Cell Environ.* 27, 51–54.
- Clarkson, D., 1984. Calcium transport between tissues and its distribution in the plant. *Plant Cell Environ.* 7, 449–456.
- Clarkson, D., 1993. Roots and the delivery of solutes to the xylem. *Philos. Trans. R. Soc., B* 341, 5–17.
- Cocker, K., Evans, D., Hodson, M., 1998. The amelioration of aluminum toxicity by silicon in higher plants: solution chemistry or an in planta mechanism? *Physiol. Plant.* 104, 608–614.
- Cornelis, J., Delvaux, B., Cardinal, D., Andre, L., Ranger, J., Opfergelt, S., 2010. Tracing mechanisms controlling the release of dissolved silicon in forest soil solutions using Si isotopes and Ge/Si ratios. *Geochim. Cosmochim. Acta* 74, 3913–3924.
- Dasch, E., 1969. Strontium isotopes in weathering profiles, deep-sea sediments, and sedimentary rocks. *Geochim. Cosmochim. Acta* 33, 1521–1552.
- Dasch, A., Blum, J., Eagar, C., Fahey, T., Driscoll, C., Siccama, T., 2006. The relative uptake of Ca and Sr into tree foliage using a whole-watershed calcium addition. *Biogeochemistry* 80, 21–41.
- de Bakker, N., Hemminga, M., Van Soelen, J., 1999. The relationship between silicon availability, and growth and silicon concentration of the salt marsh halophyte *Spartina anglica*. *Plant Soil* 215, 19–27.
- Delvigne, C., Opfergelt, S., Cardinal, D., Delvaux, B., Andre, L., 2009. Distinct silicon and germanium pathways in the soil–plant system: evidence from banana and horsetail. *J. Geophys. Res.* 114, 1–11.
- Derry, L., Kurtz, A., Ziegler, K., Chadwick, O., 2005. Biological control of terrestrial silica cycling and export fluxes to watersheds. *Nature* 433, 728–730.
- Derry, L., Pett-Ridge, J., Kurtz, A., Troester, J., 2006. Ge/Si and 87Sr/86Sr tracers of weathering reactions and hydrologic pathways in a tropical granitoid system. *J. Gechem. Explor.* 88, 271–274.

- Dijkstra, F., Van Breeman, N., Jongmans, A., Davies, G., Likens, G., 2003. Calcium weathering in forested soils and the effect of different tree species. *Biogeochemistry* 62, 253–275.
- Doucet, F., Schneider, C., Bones, S., 2001. The formation of hydroxyaluminosilicates of geochemical and biological significance. *Geochim. Cosmochim. Acta* 65, 2461–2467.
- Drouet, T., Herbauts, J., 2008. Evaluation of the mobility and discrimination of Ca, Sr, and Ba in forest ecosystems: consequence on the use of alkaline-earth element ratios as tracers of Ca. *Plant Soil* 302, 105–124.
- Duffy, C., 2008, 2009, 2010. CZO Dataset: Shale Hills—Streamflow/Discharge. <http://criticalzone.org/shale-hills/data/dataset/3613/>.
- Epstein, E., 1994. The anomaly of silicon in plant biology. *Proc. Natl. Acad. Sci. U. S. A.* 91 (11–17), 291.
- Epstein, E., 1999. Silicon. *Annu. Rev. Plant Physiol. Mol. Biol.* 50, 641–664.
- Ewers, B., Mackay, D., Samanta, S., 2007. Interannual consistency in canopy stomatal conductance control of leaf water potential across seven tree species. *Tree Physiol.* 27, 11–24.
- Fauteux, F., Remus-Borel, W., Menzies, J., Belanger, R., 2005. Silicon and plant disease resistance against pathogenic fungi. *FEMS Microbiol. Lett.* 249, 1–6.
- Flueckinger, L., 1969. Report 176, Geology of a portion of the Allensville Quadrangle, Centre and Huntingdon Counties, Pennsylvania: Bureau of Topographic and Geologic Survey, Harrisburg, PA, Commonwealth of Pennsylvania State Planning Board.
- Funk, J., Amatangelo, K., 2013. Physiological mechanisms drive differing foliar calcium content in ferns and angiosperms. *Oecologia* 173, 23–32.
- Gaines, K., Stanley, J., Meinzer, F., McCulloh, K., Woodruff, D., Chen, W., Adams, T., Lin, H., Eissenstat, D., 2015. Reliance on shallow soil water in a mixed-hardwood forest in central Pennsylvania. *Tree Physiology* (in submission).
- Gardner, T., Ritter, J., Shuman, C., Bell, J., Sasowsky, K., Pinter, N., 1991. A periglacial stratified slope deposit in the valley and ridge province of Central Pennsylvania, USA: sedimentology, stratigraphy, and geomorphic evolution. *Permafrost. Periglac. Process.* 2, 141–162.
- Garvin, C., 2006. An Exploratory Study of the Terrestrial Biogeochemical Silicon Cycle at a Forested Watershed in Northern Vermont. Cornell University, Ithaca (M.S. thesis).
- Goldschmidt, V., 1958. *Geochemistry*. Oxford University Press, London.
- Graham, C., Lin, H., 2011. Controls and frequency of preferential flow occurrence: a 175-event analysis. *Vadose Zone J.* 10, 816–831.
- Gulpin, M., Turk, S., Fink, S., 1995. Ca nutrition in conifers. *J. Plant Nutr. Soil Sci.* 158, 519–527.
- Herndon, E., Jin, L., Brantley, S., 2011. Soils reveal widespread manganese enrichment from industrial inputs. *Environ. Sci. Technol.* 45, 241–247.
- Herndon, E., Dere, A., Sullivan, P., Norris, D., Reynolds, B., Brantley, S., 2015. Landscape heterogeneity drives contrasting concentration–discharge relationships in shale headwater catchments. *Hydrol. Earth Syst. Sci.* 19, 3333–3347.
- Hogan, J., Blum, J., 2002. Tracing hydrologic flowpaths in a small forested watershed using variations in  $^{87}\text{Sr}/^{86}\text{Sr}$ ,  $[\text{Ca}]/[\text{Sr}]$ ,  $[\text{Ba}]/[\text{Sr}]$ , and  $\delta^{18}\text{O}$ . *Water Resour. Res.* 39, 1–12.
- Jarvis, S., 1987. The uptake and transport of silicon by perennial ryegrass and wheat. *Plant Soil* 97, 429–437.
- Jin, L., Ravella, R., Ketchum, B., Bierman, P., Heaney, P., White, T., Brantley, S., 2010. Mineral weathering and elemental transport during hillslope evolution at the Susquehanna/Shale Hills Critical Zone Observatory. *Geochim. Cosmochim. Acta* 74, 3669–3691.
- Jin, L., Rother, G., Cole, D., Mildner, D., Duffy, C., Brantley, S., 2011a. Characterization of deep weathering and nanoporosity development in shale—a neutron study. *Am. Mineral.* 96, 498–512.
- Jin, L., Andrews, D., Holmes, G., Lin, H., Brantley, S., 2011b. Opening the “Black Box”: water chemistry reveals hydrological controls on weathering in the Susquehanna Shale Hills Critical Zone Observatory. *Vadose Zone J.* 10, 928–942.
- Jin, L., Brantley, S., 2011. Soil chemistry and shale weathering on a hillslope influenced by convergent hydrologic flow regime at the Susquehanna/Shale Hills Critical Zone Observatory. *Appl. Geochem.* 26, S51–S56.
- Jin, L., Ogrinc, N., Yesavage, T., Hasenmueller, E., Ma, L., Sullivan, P., Kaye, J., Duffy, C., Brantley, S., 2014. The CO<sub>2</sub> consumption potential during gray shale weathering. Insights from the evolution of carbon isotopes in the Susquehanna Shale Hills critical zone observatory. *Geochim. Cosmochim. Acta* 142, 260–280.
- Jones, L., Handreck, K., 1965. Studies of silica in the oat plant. III. Uptake of silica from soils by plant. *Plant Soil* 23, 79–96.
- Kennedy, M., Chadwick, O., Vitousek, P., Derry, L., Henricks, D., 1998. Changing sources of base cations during ecosystem development, Hawaiian Islands. *Geology* 26, 1015–1018.
- Kennedy, M., Hedin, L., Derry, L., 2002. Decoupling of unpolluted temperate forests from rock nutrient sources revealed by natural  $^{87}\text{Sr}/^{86}\text{Sr}$  and  $^{84}\text{Sr}$  tracer addition. *PNAS* 99, 9639–9644.
- Kim, H., 2007. Evaluating the Effects of Forest Liming in Appalachian Watersheds: Chemistry and Multi-isotope Approaches. Pennsylvania State University: University Park (Ph.D. diss.).
- Kuntz, B., Rubin, S., Berkowitz, B., Singha, K., 2011. Quantifying solute transport at the Shale Hills Critical Zone Observatory. *Vadose Zone J.* 10, 843–857.
- Kurtz, A., 2000. Germanium/Silicon and Trace Element Geochemistry of Silicate Weathering and Mineral Aerosol Deposition. Cornell University, Ithaca (Ph.D. diss.).
- Kurtz, A., Derry, L., Chadwick, O., 2002. Germanium–silicon fractionation in the weathering environment. *Geochim. Cosmochim. Acta* 66, 1525–1537.
- Kurtz, A., Derry, L., 2004. Tracing silicate weathering and terrestrial silica cycling with Ge/Si ratios. In: Wanty, R., Seal, R. (Eds.), *Proceeding of the 11th International Symposium on Water Rock Interaction, The Netherlands*, pp. 833–836.
- Lebedeva, M., Fletcher, R., Brantley, S., 2010. A mathematical model for steady-state regolith production at constant erosion rate. *Earth Surf. Process. Landf.* 35, 508–524.
- Likens, G., Driscoll, C., Buso, D., Siccama, T., Johnson, C., Lovett, G., Fahey, T., Reiners, W., Ryan, D., Martin, C., Bailey, S., 1998. The biogeochemistry of calcium at Hubbard Brook. *Biogeochemistry* 41, 89–173.
- Lin, H., 2006. Temporal stability of soil moisture spatial pattern and subsurface preferential flow pathways in the Shale Hills catchment. *Vadose Zone J.* 5, 317–340.
- Lin, H., Kogelmann, W., Walker, C., Bruns, M., 2006. Soil moisture patterns in a forested catchment: a hydrogeological perspective. *Geoderma* 131, 345–368.
- Lin, H., Zhou, X., 2008. Evidence of subsurface preferential flow using soil hydrologic monitoring in the Shale Hills catchment. *Eur. J. Soil Sci.* 59, 34–49.
- Lucash, M., Yanai, R., Blum, J., Park, B., 2012. Foliar nutrient concentrations related to soil sources across a range of sites in the northeastern United States. *Soil Sci. Soc. Am. J.* 76, 674–683.
- Lugolobi, F., Kurtz, A., Derry, L., 2010. Germanium–silicon fractionation in a tropical, granitic weathering environment. *Geochim. Cosmochim. Acta* 74, 1294–1308.
- Lynch, J.A., 1976. Effects of Antecedent Soil Moisture on Storm Hydrographs. Pennsylvania State University: University Park (Ph.D. diss.).
- Ma, J., Takahashi, E., 1990. Effect of silicon on the growth and phosphorus uptake of rice. *Plant Soil* 126, 115–119.
- Ma, J., Yamaji, N., 2006. Silicon uptake and accumulation in higher plants. *Trends Plant Sci.* 11, 392–397.
- Ma, J., Yamaji, N., Mitani, N., Tamai, K., Konishi, S., Fujiwara, T., Katsuhara, M., Yano, M., 2007. An efflux transporter of silicon in rice. *Nature* 448, 209–212.
- Ma, L., Chabaux, F., Pelt, E., Blaes, E., Jin, L., Brantley, S., 2010. Regolith production rates calculated with uranium-series isotopes at Susquehanna/Shale Hills Critical Zone Observatory. *Earth Planet. Sci. Lett.* 297, 211–225.
- Ma, L., Jin, L., Brantley, S., 2011a. Geochemical behaviors of different element groups during shale weathering at the Susquehanna/Shale Hills Critical Zone Observatory. *Appl. Geochem.* 26, S89–S93.
- Ma, L., Jin, L., Brantley, S., 2011b. How mineralogy and slope aspect affect REE release and fractionation during shale weathering in the Susquehanna/Shale Hills Critical Zone Observatory. *Chem. Geol.* 290, 31–49.
- Ma, L., Chabaux, F., West, N., Kirby, E., Jin, L., Brantley, S., 2013. Regolith production and transport in the Susquehanna Shale Hills Critical Zone Observatory, part 1: insights from U-series isotopes. *J. Geophys. Res. Earth Surf.* 118, 722–740.
- Ma, L., Teng, F., Jin, L., Ke, S., Yang, W., Gu, H., Brantley, S., 2015. Magnesium isotope fractionation during shale weathering in the Shale Hills Critical Zone Observatory: accumulation of light Mg isotopes in soils by clay mineral transformation. *Chem. Geol.* 397, 37–50.
- Marschner, P., 2012. *Mineral Nutrition of Higher Plants*. third ed. Academic Press, London.
- Martin, F., Ildefonse, P., Hazemann, J., Petit, S., Grauby, O., Decarreau, A., 1996. Random distribution of Ge and Si in synthetic talc: an EXAFS and FTIR study. *Eur. J. Mineral.* 8, 289–299.
- McLaughlin, S., Wimmer, R., 1999. Calcium physiology and terrestrial ecosystem processes. *New Phytol.* 142, 373–417.
- McNair, J., 1932. The interrelation between substances in plants: essential oils and resins, cyanogens and oxalate. *Am. J. Bot.* 19, 255–272.
- Meinzer, F., Woodruff, D., Eissenstat, D., Lin, H., Adams, T., McCulloh, K., 2013. Above- and belowground controls on water use by trees of different wood types in an eastern US deciduous forest. *Tree Physiol.* 33, 345–356.
- Miller, E., Blum, J., Friedland, A., 1993. Determination of soil exchangeable cation loss and weathering rates using Sr isotopes. *Nature* 362, 438–441.
- Miller, S., Sak, R., Kirby, E., Bierman, P., 2013. Neogene rejuvenation of central Appalachian topography: evidence for differential rock uplift from stream profiles and erosion rates. *Earth Planet. Sci. Lett.* 369, 1–12.
- Mitani, N., Ma, J., 2005. Uptake system of silicon in different plant species. *J. Exp. Bot.* 56, 1255–1261.
- Mortlock, R., Froelich, P., 1987. Continental weathering of germanium: Ge/Si in the global river discharge. *Geochim. Cosmochim. Acta* 51, 2075–2082.
- Mortlock, R., Froelich, P., 1996. Determination of germanium by isotope dilution-hydride generation inductively coupled plasma mass spectrometry. *Anal. Chim. Acta* 332, 277–284.
- Murnane, R., Stallard, R., 1990. Germanium and silicon in rivers of the Orinoco drainage basin. *Nature* 344, 749–752.
- National Atmospheric Deposition Program (NADP), 2013. Seasonal Precipitation-Weighted Mean Concentrations for PA-15. <http://nadp.sws.uiuc.edu>.
- Naithani, K., Baldwin, D., Gaines, K., Lin, H., Eissenstat, D., 2013. Spatial distribution of tree species governs the spatio-temporal interaction of leaf area index and soil moisture across a forested landscape. *PLoS One* 8, 1–12.
- National Oceanographic and Atmospheric Administration (NOAA), 2007a. U.S. divisional and station climatic data and normals: Asheville, North Carolina, U.S. Department of Commerce, National Oceanic and Atmospheric Administration, National Environmental Satellite Data and Information Service, National Climatic Data Center. <http://cdo.ncdc.noaa.gov/CDO/cdo>.
- Parr, J., Dolic, V., Lancaster, G., Boyd, W., 2001. A microwave digestion method for the extraction of phytoliths from herbarium species. *Rev. Palaeobot. Palynol.* 116, 203–212.
- Pett-Ridge, J., Derry, L., Barrows, J., 2009. Ca/Sr and  $^{87}\text{Sr}/^{86}\text{Sr}$  ratios as tracers of Ca and Sr cycling in the Rio Icacos watershed, Luquillo Mountains, Puerto Rico. *Chem. Geol.* 267, 32–45.
- Poszwa, A., Dambrine, E., Pollier, B., Atteia, O., 2000. A comparison between Ca and Sr cycling in forest ecosystems. *Plant Soil* 225, 299–310.
- Qu, Y., Duffy, C., 2007. A semidiscrete finite volume formulation for multiprocess watershed simulation. *Water Resour. Res.* 43, 1–18.
- Raven, J., 1983. The transport and function of silicon in plants. *Biol. Rev.* 58, 179–207.
- Raven, J., 2003. Cycling silicon—the role of accumulation in plants. *New Phytol.* 158, 419–421.

- Runia, L., 1987. Strontium and calcium distribution in plants: effects on paleodietary studies. *J. Archeol. Sci.* 14, 599–608.
- Schlesinger, W., 1997. *Biogeochemistry: An Analysis of Global Change*. second ed. Academic Press, San Diego.
- Scribner, A., Kurtz, A., Chadwick, O., 2006. Germanium sequestration by soil: targeting the roles of secondary clays and Fe-oxyhydroxides. *Earth Planet. Sci. Lett.* 243, 760–770.
- Shand, P., Darbyshire, D., Goody, D., Haria, A., 2007.  $^{87}\text{Sr}/^{86}\text{Sr}$  as an indicator of flowpaths and weathering rates in the Plynlimon experimental catchments, Wales, U.K. *Chem. Geol.* 236, 247–265.
- Shannon, R., 1976. Revised effective ionic radii and systematic studies of interatomic distances in halides and chalcogenides. *Acta Crystallogr. A* 32, 751–767.
- Sommer, M., Kaczorek, D., Kuzyakov, Y., Breuer, J., 2006. Silicon pools and fluxes in soils and landscapes—a review. *J. Plant Nutr. Soil Sci.* 169, 310–329.
- Sparks, J., Chandra, S., Derry, L., Parthasarathy, M., Daugherty, C., Griffin, R., 2010. Subcellular localization of silicon and germanium in grass root and leaf tissues by SIMS: evidence for differential and active transport. *Biogeochemistry* 104, 237–249.
- Street-Perrott, F., Barker, P., 2008. Biogenic silica: a neglected component of the coupled global continental biogeochemical cycles of carbon and silicon. *Earth Surf. Process. Landf.* 33, 1436–1457.
- Takagi, K., Lin, H., 2012. Changing controls of soil moisture spatial organization in the Shale Hills Catchment. *Geoderma* 173–174, 289–302.
- Tardieu, F., Simonneau, T., 1998. Variability among species of stomatal control under fluctuating soil water status and evaporative demand: modeling isohydric and anisohydric behaviors. *J. Exp. Bot.* 49, 419–432.
- Thomas, E., Lin, H., Duffy, C., Sullivan, P., Holmes, G., Brantley, S., Jin, L., 2013. Spatiotemporal patterns of water stable isotope compositions at the Shale Hills Critical Zone Observatory: linkages to subsurface hydrologic processes. *Vadose Zone J.* 12, 1–16.
- Veresoglou, D., Barbayiannis, N., Matsi, T., Anagnostopoulos, C., Zalidis, G., 1996. Shoot Sr concentrations in relation to shoot Ca concentrations and to soil properties. *Plant Soil* 178, 95–100.
- Watmough, A., Dillon, P., 2003. Calcium losses from a forested catchment in South-Central Ontario, Canada. *Environ. Sci. Technol.* 37, 3085–3089.
- West, H., Davies, S., Morgan, J., Herbert, R., 2001. The relationship between Sr and Ca accumulation in the major constituents of a terrestrial community resident on a celestic (SrSO<sub>4</sub>) soil in S.W. England. *Eur. J. Soil Biol.* 37, 333–336.
- West, N., Kirby, E., Bierman, P., Rood, D., 2011. Preliminary estimates of regolith generation and mobility in the Susquehanna Shale Hills Critical Zone Observatory, Pennsylvania, using meteoric  $^{10}\text{Be}$ . *Appl. Geochem.* 26, S146–S148.
- White, P., 2001. The pathways of calcium movement to the xylem. *J. Exp. Bot.* 52, 891–899.
- White, P., Whitting, S., Baker, A., Broadley, M., 2002. Does zinc move apoplastically to the xylem in roots of *Thlaspi caerulescens*? *New Phytol.* 153, 199–211.
- White, P., Broadley, M., 2003. Calcium in plants. *Ann. Bot.* 92, 487–511.
- Whitney, P., Hurley, P., 1964. The problem of inherited radiogenic strontium in sedimentary age determinations. *Geochim. Cosmochim. Acta* 28, 425–436.
- Wolterbeek, H., van Luijpen, J., de Bruin, M., 1984. Non-steady state xylem transport of fifteen elements into the tomato leaf as measured by gamma-ray spectroscopy: a model. *Physiol. Plant.* 61, 599–606.
- Wytenbach, A., Furrer, V., Tobler, L., 1995. The concentration ratios plant to soil for stable elements Cs, Rb, and K. *Sci. Total Environ.* 173, 361–367.
- Wubbels, J., 2010. *Tree Species Distribution in Relation to Stem Hydraulic Traits and Soil Moisture in a Mixed Hardwood Forest in Central Pennsylvania*. Pennsylvania State University: University Park (M.S. Thesis).
- Yamaji, N., Mitani, N., Ma, J., 2008. A transporter regulating silicon distribution in rice shoots. *Plant Cell* 20, 1381–1389.